THE UNIVERSITY OF OKLAHOMA

GRADUATE COLLEGE

INFLUENCE OF CATALYST PARTICLE SIZE ON REACTION KINETICS: HYDROGENATION OF ETHYLENE ON NICKEL

A DISSERTATION

SUBMITTED TO THE GRADUATE FACULTY

in partial fulfillment of the requirements for the

degree of

DOCTOR OF PHILOSOPHY

BY

JAMES WILLIAM FULTON

Norman, Oklahoma

1964

INFLUENCE OF CATALYST PARTICLE SIZE ON REACTION KINETICS:
HYDROGENATION OF ETHYLENE ON NICKEL

A DISSERTATION

APPROVED FOR THE SCHOOL OF CHEMICAL ENGINEERING

BY

Orrin K. Crosser

R L Huntington

F. A. Murphy

C. M. Shepherd

F. M. Townsend

ACKNOWLEDGEMENTS

Many generous people contributed to this study. Special appreciation is extended to Dr. Orrin K. Crosser, who guided this work through its final stages. His helpful suggestions and unfailing interest will always be remembered. Dr. J. E. Powers, Dr. R. H. Perry, Dr. C. M. Sliepcevich, Dr. R. L. Huntington, and Dr. G. W. Murphy gave graciously of their time during the author's graduate work.

The author is indebted to several organizations for their financial support during the period of graduate study and this investigation: Phillips Petroleum Company, Atlantic Refining Company, National Science Foundation, Ford Foundation, and the University of Oklahoma.

The contributions of my wife, Mary Frances, are more numerous than I can count and more important than I can express.

James William Fulton

TABLE OF CONTENTS

LIST OF ILLUSTRATIONS

INFLUENCE OF CATALYST PARTICLE SIZE ON REACTION KINETICS: HYDROGENATION OF ETHYLENE ON NICKEL

CHAPTER I

INTRODUCTION

> The most challenging problem in the unknown fringes of science and chemical technology today is to establish scientific principles of catalyst activity. . . . Conclusive scientific principles involved in the selection of a catalyst and factors determining catalyst activity still remain obscure.
>
> Olaf A. Hougen
> Award Address, American Chemical Society Award in Industrial and Engineering Chemistry, 1961 (29)

> No development would have a greater impact on the chemical industry than a real engineering exploitation of catalysis.
>
> Report on Dynamic Objectives for Chemical Engineering, 1961: American Institute of Chemical Engineers (1)

Advances in the chemical industry would be greatly accelerated if catalysis could be better understood. Yet today the principles of catalysis remain the weak link in the chain of chemical processing. The practical application of catalysis is clear: scientific selection of solid catalysts; interpretation of experimental data; optimum design and operation of catalytic reactors. Before the application, however, must come discovery and understanding.

In this spirit, the research reported here was directed toward

one facet of catalysis--a study of the influence of catalyst particle size on the reaction process of a surface catalyzed reaction.

The reaction system chosen for this study was the hydrogenation of ethylene to ethane on a nickel catalyst. This reaction system has several assets which recommend its use. First, the reaction proceeds without any side reactions. This characteristic reduces the complexity of the kinetic data and allows the influence of each variable on the catalytic activity to be more easily isolated. Second, the hydrogenation does not occur to a measurable degree in the absence of a catalyst. Thus, homogeneous, wall-catalyzed and other reactions need not be considered. Third, conversion of any amount may be obtained at moderate operating conditions. Fourth, there is much information available which discusses the kinetics of this reaction. This information is most helpful in looking beyond the reaction mechanism to find the influence of the solid catalyst.

The rate of a heterogeneous catalyzed reaction is determined by both the chemical reaction kinetics at the surface and by the rate of heat and mass transfer to this surface. When the reaction is operating at a steady state, the number of moles of a component destroyed at the catalyst surface by the chemical reaction is exactly equal to the number of moles of that component transported to the surface by convective or molecular diffusion. Likewise, the heat generated by the reaction must equal the heat removed by convective, conductive, and radiant heat exchange. Increasing the size of a catalyst pellet increases the area for heat transfer, mass transfer, and chemical reaction. Increasing pellet size, however, not only changes the area through which these transport mechanisms act but also changes the heat and mass transfer

coefficients. This variation in behavior between the transport phenomena and chemical reaction with changing particle size causes a change in character of the reaction kinetic data. Changing temperature and concentration have varying effects on the reaction rate. Reaction rates generally change linearly or nearly linearly with changes in concentration, but they change exponentially with changes in temperature. Catalyst surface temperatures as much as 420°C above that of the bulk gas temperature (46) may occur. This higher temperature may promote shifts in reaction mechanism, undesirable side reactions such as coking, or other changes in the catalyst behavior and properties.

In order to obtain an accurate picture of catalyst activity and reaction kinetics, it is necessary to study the behavior of the reaction at the catalyst surface. Experimentally, it is difficult or impossible to measure temperatures and chemical concentrations directly on the surface of a catalyst pellet. Generally one can measure only bulk gas temperatures and concentrations. Therefore the influence of heat and mass transfer phenomena between the bulk gas phase and the catalyst surface must be taken into consideration. These phenomena are a function of the catalyst particle size, and this function is of critical influence. Thus, small changes in the size of the catalyst particle may have a profound effect upon the behavior of the reaction. The purpose of this study is to determine the precise character of this effect.

CHAPTER II

REVIEW OF PREVIOUS WORK

The review of the previous work done on the concepts used in this paper may be divided into two general areas: reaction kinetics studies of the hydrogenation of ethylene on nickel catalysts, and heat and mass transfer studies for particles in a packed bed.

Reaction Kinetics

Much experimental work has been done on the reaction kinetics of the hydrogenation of ethylene, and several reaction mechanisms have been proposed in an effort to explain the observed experimental phenomena. The greatest controversy concerning the kinetics of this reaction is between two proposed mechanisms, "associative" and "dissociative," for the adsorption of ethylene on the nickel catalysts (33) (58). The rate expression for either mechanism is the same, however, and this common expression can be used in catalyst studies. Therefore, the details of these mechanism studies will not be considered, and only the general behavior pattern noted.

Some of the more important papers which discuss this catalytic reaction begin with Beeck (5). He studied the hydrogenation rate over evaporated porous metal films of the transition elements and correlated the data with the d-character of the metallic single bond. At the same

time, Twigg (58) used infra-red spectroscopic examination as proof that the hydrogen is first dissociated into atoms on the catalyst during the hydrogenation reaction. Although his proposed reaction mechanism has been disputed more recently (42), his pioneering work gave insight into the behavior of the catalyst. Jenkins and Rideal's studies (33) (34) examined the adsorption of ethylene on nickel films. They found that ethylene undergoes dissociative chemisorption to form an adsorbed acetylenic complex which produces a partly "carbided" catalyst surface. Laidler and Townshend (36) found that the order of introduction of the reactant gases to the nickel film was important to the subsequent rate of reaction. The greatest rate was obtained when hydrogen was introduced first; a lower rate resulted when hydrogen and ethylene were introduced simultaneously. The lowest rate occurred when ethylene was introduced first. In the present study hydrogen was always introduced first. Crawford, Roberts and Kemball (15) found that the kinetics and activation energy for the hydrogen of ethylene on nickel films are not influenced by the temperature used to sinter the films.

Several excellent and general reviews of the catalytic hydrogenation of ethylene studies are available. Eley (17) has a review of the more prominent theories, including the theory of the adsorbed film, the parahydrogen conversion on nickel, and the stereochemistry of hydrogenation. A paper by Hoelscher, Poynter, and Weger (27) reviews the literature on the hydrogenation of the olefin hydrocarbons over solid catalysts. Their survey includes theoretical and experimental reports on adsorption and transfer of heat and mass as well as kinetic studies of the reaction mechanism. A recent book by Bond (7) covers the general field of

catalysis by metals. His book includes a chapter on the hydrogenation of olefins which summarizes the experimental results of ethylene hydrogenation on nickel. His summary for this energy of activation determined by various workers is given in Table I.

TABLE I

ETHYLENE HYDROGENATION ENERGY OF ACTIVATION: NICKEL CATALYSTS

Catalyst Form	Energy of Activation (kcal/gm-mole)	Temperature Range (°C)
Film	10.7	-80 to 150
Film	8.0	0 to 96
Film	10.2	20 to 150
Film	7	-100 to-120
Wire	14	60 to 100
Wire	4.6	0 to 17
Wire	8.2	60 to 110
Foil	3.2	30 to 200
Foil	5	400 to 600
Powder	6	-78 to 0
Powder	7.5	-70
on SiO_2	8.4	-78 to 0
on Al_2O_3	11.6	30 to 80

Although none of the theories advanced for this reaction mechanism has been proven to be conclusively true, there are some areas of

general agreement. First, there is general agreement that the reaction is unaffected by the presence of ethane, other than through its action as an inert diluent (17)(33). Furthermore, there seems to be a reaction mechanism shift between 150°C to 200°C. The reaction mechanism at the lower temperatures is generally correlated as first order with respect to the hydrogen partial pressure (5)(20) but has also been correlated as first order with respect to the partial pressures of both hydrogen and ethylene (43). It seems reasonable that Beeck's value for the energy of activation at the lower temperatures, $\Delta H^* = 10.7$ kcal/gm-mole, is probably the most accurate, since it was taken over a range of -80 to 150°C. Pauls, Comings, and Smith's (42) value of $\Delta H^* = 11.6$ kcal/gm-mole might also be reasonable for purposes of comparison, since it was obtained using a nickel-on-alumina catalyst similar to the one used in this study. The mechanism at the higher temperatures is generally correlated as first order with respect to the partial pressures of both hydrogen and ethylene (18). A value for the energy of activation above 150°C is difficult to gather from the literature values. Most researchers find values below 3.4 kcal/gm-mole (58). For ethylene pressures less than a few millimeters of mercury at high temperatures, the reaction can be correlated as first order with respect to ethylene and independent of the hydrogen concentration (18).

Transfer Processes

Heat and mass transfer processes for a catalyst pellet may be divided into two categories: those processes which occur inside the pellet, and those which occur in the stagnant gas film surrounding the pellet.

A review of these processes has been published recently by Hougen (29). Mathematical expressions describing the overall behavior of packed bed reactors are given and solved numerically by Park (41) and von Rosenberg (59). Textbooks by Hougen and Watson (31) and Smith (55) consider general heat and mass transfer correlations for a packed bed.

Much interest lately has centered around the relation between catalytic activity as influenced by heat and mass transfer within porous solid catalysts (38)(51)(57)(60). The pioneering paper on pore diffusion in isothermal catalysts was by Thiele (56). He defined an effectiveness factor to show the role of pore length on the reaction rate. Wheeler (61) later reviewed the entire problem of the influence of catalyst pores on reaction rates and selectivity. Schilson set up and numerically solved the mathematical equations for heat and mass transfer within a catalyst pellet for his Ph.D. thesis (51). Subsequently he and Amundson published two papers on this study (52)(53). Prater (45) derived a simple expression for the temperature gradient within a pellet. Mingle and Smith (38) studied the influence of varying pore diameters and proposed microeffectiveness and macroeffectiveness factors. Aris (2) considered the modifications which must be made on pore diffusion results for irregularly shaped particles.

Three recent papers present solutions of the non-linear differential equations for mass and energy balances inside a porous catalyst pellet. These papers consider the reactivity behavior of the pellets subject to both internal mass concentration gradients as well as temperature gradients in endothermic and exothermic reactions. Tinkler and Metzner (57) solved the equations on an analog computer, Weisz and Hicks

(60) on an IBM 7090, and Carberry (10) on an IBM 650. Chu and Hougen (13) have discussed the effect of adsorption on the effectiveness factor.

Shifting from studies of effects occurring inside the catalyst pellet to those which consider external surface effects, we find that heat and mass transfer through a stagnant gas film rather than through pores becomes important. Theoretical approaches to the influence of operating variables on this gas film surrounding the pellet have not been useful to date. The boundary-layer of a gas flowing past a sphere with heat and mass transfer between the gas and sphere is extremely complex. Five recent papers which have offered models of this system have been presented by Carberry (9), Kusik and Happel (35), Hoelscher (28), Rosner (49), and Pfeffer and Happel (44).

Although the system of heat and mass transfer through a gas film in a packed bed is complex, there have been extremely useful correlating equations developed over the past thirty years. Chilton and Colburn (12) applied the principles for fluid friction to heat and mass transfer. They defined j-factors for several systems, including adsorption of water from air flowing across a single cylinder. The j-factor occupies the same role in heat and mass transfer that the friction factor occupies in friction correlations.

$$j_H = \left(\frac{h_G}{C_{p_M} G_M}\right)\left(\frac{C_{p_m}\mu}{k}\right)_f^{2/3} \qquad \text{(II-1)}$$

$$j_D = \left(\frac{k_{G_i} P_f}{G_M}\right)\left(\frac{\mu}{\rho_g D_i}\right)_f^{2/3} \qquad \text{(II-2)}$$

where j_H = heat transfer number, dimensionless

j_D = mass transfer number, dimensionless

h_G = gas phase heat transfer coefficient, cal/cm^2 hr ^oK

C_{p_m} = heat capacity per unit mass at constant pressure, cal/gm ^oK

C_{p_M} = molal heat capacity at constant pressure, cal/gm-mole ^oK

μ = viscosity of the gas, gm/cm sec

k = thermal conductivity, cal/cm^2 hr ^oK

k_G = gas phase mass transfer coefficient, gm-moles/cm^2 hr

ρ_g = average density of gas phase, gm/cm^3

D_i = gas phase diffusion coefficient of component i, cm^2/sec

G_M = superficial molal velocity of the gas based upon the total crossectional area of the bed, gm-moles/cm^2 hr

p_f = pressure factor, defined as the logarithmic mean value of the partial pressure over the boundary limits of the gas film, atm.

Gamson, Thodos, and Hougen (23) applied a similar analogy to heat and mass transfer in the flow of gases through granular beds. They used ten different solids, five spherical and five cylindrical in shape, which had a variety of dimensions and covered a wide range of densities and porosities. For these measurements, water was evaporated from catalyst carriers into a stream of air. These data were correlated with the Reynolds number:

$$j_D \text{ and } j_H \propto \left(\frac{d_p G_m}{\mu} \right)^n$$

where d_p = particle diameter, cm

G_m = superficial mass velocity of the gas, gm/cm^2 hr

The experimental measurements of j_D-factor dependence on the Reynolds number can be divided into two classes. The first class

correlates data taken from a system using evaporation of a liquid from porous pellets. The second class correlates data using a gas film only, by sublimating solid napthalene pellets. It has been generally assumed in the literature that the j_D-factor correlations for these two classes should be the same. This assumption, however, does not seem reasonable from a mechanistic point of view, and the literature data show the error of this assumption. A porous sphere with an evaporating liquid film will have a different interfacial surface area than the geometric surface area, on which the calculation of the transfer coefficients are based. Also, capillary action of the porous pellets, distortion of the liquid film by the gas momentum, vapor-liquid film effects, and other factors due to the presence of a liquid would modify the mass transfer correlations. These correlations based on the presence of a liquid film are useful in the design of vapor-liquid contacting equipment, such as absorbers, but they would not be directly applicable to systems not having a liquid film. A few of the more prominent j_D-factor correlations based on the presence of a gas-liquid film are given below:

$$j_D = 16.8\ (Re)^{-1} \qquad Re < 40$$

$$j_D = 0.989\ (Re)^{-0.41} \qquad Re > 350 \qquad (23)$$

$$j_D = 1.82\ (Re)^{-0.51} \qquad 45 < Re < 350 \qquad (62)$$

$$j_D = 1.625\ (Re)^{-0.507} \qquad Re < 120$$

$$j_D = 0.687\ (Re)^{-0.327} \qquad Re > 120 \qquad (39)$$

Most of the j-factor correlations have been reviewed by Ramaswami in his recent Ph.D. thesis (46). He correlated the heat and mass transfer factors with a modified Reynolds number,

$$Re = \frac{G_m}{a_v \phi \mu}$$

where G_m = superficial mass velocity of the gas based upon the total crossectional area of the bed, gm/cm^2 hr

a_v = surface area of the particles per unit volume of the bed, cm^2/cm^3

ϕ = particle shape factor as defined by Gamson (23) equal to the ratio of actual external surface area available for mass transfer to the total external surface area, dimensionless

His correlations are as follows:

$$j_D = 0.84\ (Re)^{-0.51} \qquad \text{for } 0.01 < Re < 50$$

$$j_D = 0.57\ (Re)^{-0.41} \qquad \text{for } 50 < Re < 1000$$

$$j_H = 1.077\ j_D$$

Data taken using a gas film only, without the presence of a liquid, would not have the added complexity introduced by the liquid film. The j_D-factor correlations for these gas-film studies were generated by sublimating napthalene spheres in air or CO_2 streams (3)(14)(32)(48) and decomposing H_2O_2 vapor on nickel spheres (50). j_H-factor correlations for packed beds were developed by dielectrically heating plastic particles (19) and electrically heating metal spheres (4)(16)(25). A summary of the j-factor correlations with a gas film only are given below:

$j_D = 0.18(Re)^{-0.376}$	$1 < Re < 400$	(32)(48)
$j_D = (Re)^{-0.35}$	$1 < Re = \left(\frac{d_p G_m}{(1-\epsilon)\mu}\right) < 30$	(14)
$j_D = 0.66(Re)^{-0.46}$	$0.17 < Re < 250$	(3)
$j_D = 0.724(Re)^{-0.34}$	$15 < Re < 161$	(50)
$j_D = 0.606(Re)^{-0.309}$ (including axial mixing)	$400 < Re < 10{,}000$	(8)

$$j_D = 0.506(Re)^{-0.293} \qquad 400 < Re < 10{,}000 \qquad (8)$$
(Omitting axial mixing)

$$j_H = 0.235(Re)^{-0.35} \qquad 1 < Re < 18 \qquad (19)$$

$$j_H = 0.918(Re)^{-0.29} \qquad 200 < Re < 10{,}400 \qquad (4)$$

$$j_{H_o} = \frac{0.535}{(Re)^{0.3} - 1.6} \quad \text{for} \quad \frac{\sqrt{a_p}}{D_t} \to 0$$

$$100 < Re = \left(\frac{a_p G_m}{(1-\epsilon)\phi\mu}\right) < 10{,}000 \qquad (25)$$

$$\frac{j_H}{j_{H_o}} = 1 + 10.73 \frac{\sqrt{a_p}}{D_t} (Re)^{-0.384} \quad \text{for} \quad \frac{\sqrt{a_p}}{D_t} \gg 0$$

$$j_H = 0.992(Re)^{-0.34} \qquad 15 < Re < 161 \qquad (50)$$

$$j_H = 0.584(Re)^{-0.30} \qquad 500 < Re < 50{,}000 \qquad (16)$$

Chu, Kalil, and Wetteroth (14) combined their gas film data with the liquid-gas film data of Gamson, Thodos, and Hougen (23), Wilkie and Hougen (62), McCune and Wilhelm (39), and others. They reported that their data agreed with that of the liquid-gas film correlations given earlier. A correlation of their gas film data alone, however, gives a correlation of $j_D = (Re)^{-0.35}$, in closer agreement with the results for gas film alone.

A look at the gas film j-factor correlations shows that the exponent on the Reynolds number varies between 0.29 to 0.35. The coefficient multiplying the Reynolds number varies between approximately 0.2 and 1.0. Several investigators have shown that this multiplying coefficient is a function of system variables (25)(32)(48). The unreliability of this coefficient is the weakest point in these transport phenomena correlations.

The relationship between the heat transfer factor, j_H, and the

mass transfer factor, j_D, was demonstrated by Satterfield and Resnick (50). They decomposed hydrogen peroxide on nickel spheres, and found the ratio $j_H/j_D = 1.37$.

The heat and mass transfer correlations discussed above are tools with which to calculate catalyst surface temperatures and concentrations. The behavior of the process occurring at the catalyst surface was discussed by Frank-Kamenetskii (21). He applied the ideas and methods which have been useful in the theory of thermal ignition in homogeneous reactions to the problem of the increased catalyst surface temperature (thermal regime) of heterogeneous exothermal reactions. He noted that the rate of a heterogeneously catalyzed reaction was determined both by the true chemical reaction kinetics and by the rate of supply of reactants to the surface through molecular or convective diffusion. At low temperatures, as long as the rate of reaction is small compared with the rate of diffusion, the overall rate of reaction is determined by the chemical reaction kinetics at the surface (kinetic region, or lower thermal regime) and increases exponentially with the temperature according to Arrhenius' law. This temperature increase, however, can continue only until the rate of the reaction becomes comparable with the rate of the diffusion. From that transition point, the process will pass into the diffusional region (upper thermal regime), where its rate is determined by the rate of diffusion.

For Frank-Kamenetskii's proposed mechanism of heat and mass transfer, three stationary thermal states are possible: the lower state or reaction kinetics region, the upper state or diffusional region, and the unstable intermediate state. Ignition of the surface represents a

discontinuous transition from the lower to the upper stationary thermal regime. The reverse transition from the upper to the lower regime also takes place discontinuously at the critical condition of extinction. Therefore, in an exothermic heterogeneous reaction, there can be two stationary thermal states: the kinetic region where there is a small temperature rise between the bulk gas and the catalyst surface (lower thermal regime); the diffusional region where there is a large temperature rise. Passage from one regime to another occurs discontinuously at the critical conditions of ignition and extinction at the catalyst surface. For a more detailed discussion of Frank-Kamenetskii's study, see Appendix A.

From the preceding discussion we see that several areas of study have developed which are applicable to heterogeneous reactions in a packed bed: reaction kinetics studies, heat and mass transfer correlations, and mathematical and theoretical developments. No study has been reported, however, which considers the influence of particle size on the kinetics of a reaction occurring on the external surface of a catalyst. The literature indicates that the influence of catalyst particle size may be important for this system, but no experimental work has been conducted to study this influence. All but one of the heat and mass transfer correlations for a packed bed consider non-reacting systems. The only exception is that of Satterfield and Resnick (50), who decomposed hydrogen peroxide on nickel spheres. They did not, however, vary the size of their catalyst spheres.

Therefore, it would seem important, in the area of heterogeneous catalysis, to gather and study data demonstrating the influence of catalyst particle size on the behavior of the reaction process.

CHAPTER III

APPARATUS

The apparatus used in this study may be divided into four units: feed system, reactor, temperature measuring system, and gas analysis system. A schematic diagram of the apparatus is shown in Figure 1 and a detailed diagram of the reactor in Figure 2. Except for tygon tubing transporting room temperature hydrogen and ethylene gases, all equipment is glass, with ground-glass joints used for all connections. Silicone lubricant was used on glass connections at room temperature. This apparatus operated at atmospheric pressure.

Feed System

Hydrogen and ethylene gases were fed from commerical cylinders with constant pressure regulators and pressure reducing needle valves. Their flow was measured by capillary tube flowmeters. Triethylene glycol was used as the manometric fluid because of its low vapor pressure at room temperature (0.1 mm Hg at 176^{o}F). The flowmeters were calibrated against a rising soap-film flowmeter. The hydrogen and ethylene feed temperatures were recorded continuously during the calibrations as well as during the reaction runs.

A Deoxo catalytic purifier for electrolytic hydrogen was installed in the hydrogen line to reduce any traces of oxygen to water. A

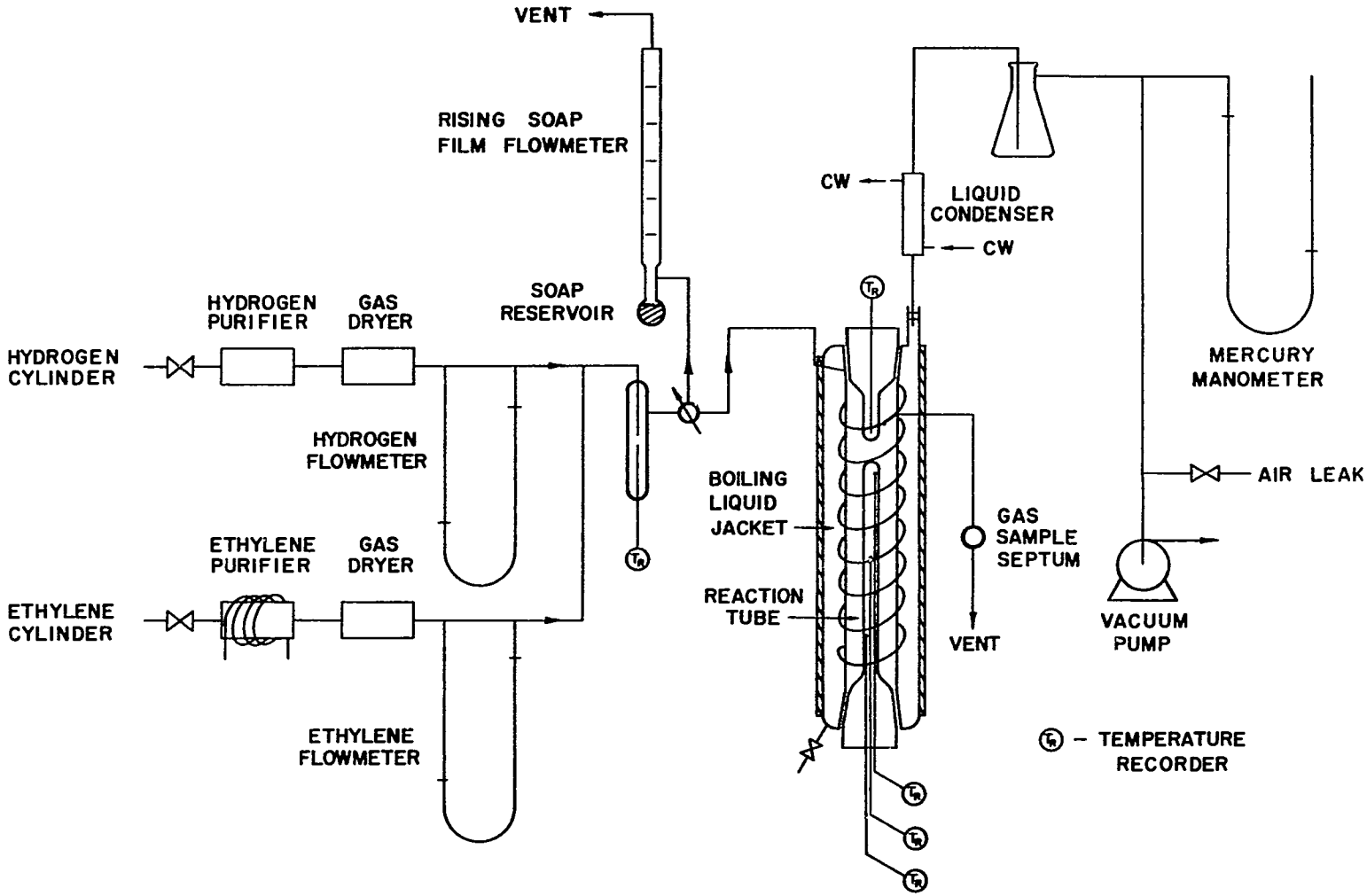

Figure 1 - Flow Diagram of Experimental Apparatus

heated Model C Deoxo Purifier for removal of oxygen and sulfur was installed in the ethylene line.

Both gas streams passed from their purifiers through Drierite drying tubes, in order to remove moisture.

The gases were thoroughly mixed in a mixing chamber before being fed to the preheater.

Reactor

The reactor was designed with the primary purpose of maintaining an accurate and isothermal temperature level. The entering gases passed through a preheater coil of 7 mm glass tubing which wrapped around the reaction tube and emptied into it at the bottom. From the bottom of the reactor the reactants passed up through the reactor tube containing the catalyst bed and out the top of the reactor. The preheater coil served to bring the reactants up to reaction temperature before they entered the catalyst bed. The preheater coil and reaction tube were in a boiling liquid jacket. The liquid jacket, in turn, was surrounded by an insulated, electrically heated resistance wire coil. The temperature of the boiling liquid was controlled by regulating the vacuum above it.

A glass thermowell rose through the middle of the reaction tube and thus through the middle of the catalyst bed. It was fitted on a ground-glass joint, which allowed an opening at the bottom of the reactor so that the catalyst beds could be changed without moving the reactor and other apparatus. Another thermowell was fixed overhead in the gases passing out of the reactor. This thermowell was fitted on a ground-glass joint, permitting easy loading of the reactor.

The reactor bed was packed in a particular way in order to hold

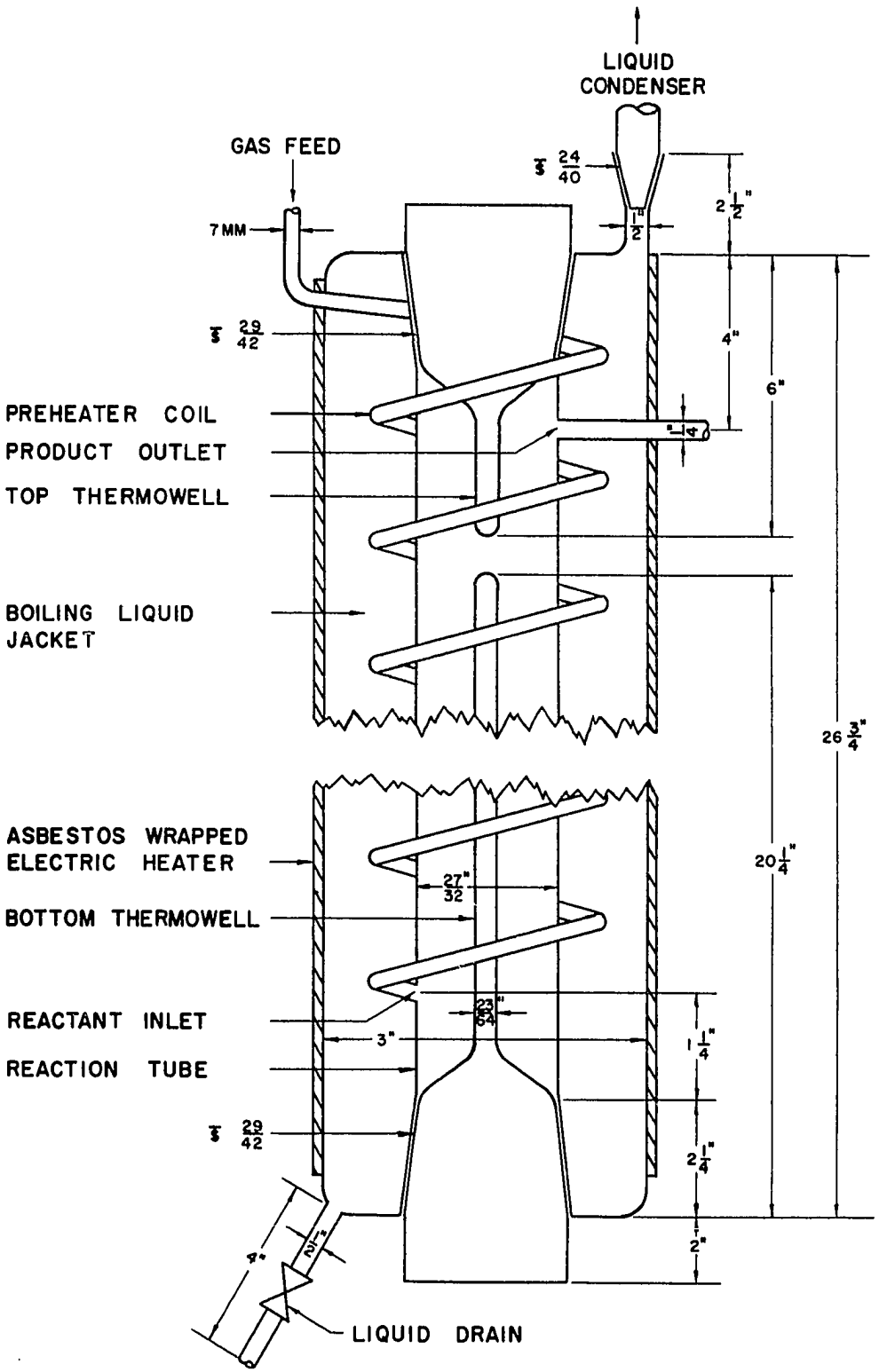

Figure 2 - Reactor Diagram

isothermal conditions and maintain the bed fixed. The method of packing is discussed in Chapter V.

Temperature Measuring System

All temperatures at the thermocouple points indicated in Figure 1 were sensed by iron-constantan thermocouples inserted in glass thermowells.

Three thermocouples were inserted in the thermowell rising up through the reactor, as shown in Figures 1 and 3. One was at the bottom of the reactor bed, another in the middle, and a third at the top. They were separated by glass wool packing and served to indicate the temperature profile up the reactor bed. A thermocouple in the top thermowell of the reactor measured the temperature of the effluent gas. Thermocouples also measured the gas feed temperature and room temperature. Each temperature sensed was recorded every three minutes on a strip chart by a Brown "Electronik" Multipoint Recording Potentiometer, Model No. 153X60P12-X-31, with a range of 0 to 500°F.

Product Analysis System

A vapor phase, partition chromatograph, built and modified in conjunction with previous research projects (27)(39), was used to analyze the reacting and product mixtures. A four-foot copper tube, one-fourth inch in diameter, packed with finely divided silica gel, constituted the column used for the gas analysis. The column temperature was maintained at 208°F and the gas thermal-conductivity cell temperature at 165°F, with a helium flow of 150 cc per minute. The analysis was determined by comparing the peak heights of the elution curves obtained for the reaction

gas samples to those obtained from the standard gas mixtures. Six different compositions of gas samples were used as standards.

In the procedure for obtaining the standard gas samples, a 500 cubic inch stainless steel cylinder was evacuated. Ethylene, ethane, and hydrogen were added in succession to the cylinder in amounts determined by absolute pressure measurements taken before and after each gas addition. The absolute pressure measurements were obtained from a mercury manometer connected to the cylinder.

After addition of the gases, the cylinders which contained about 100 ml of 0.8 mm glass beads were shaken vigorously to assure complete mixing.

A one-cubic centimeter gas sample was used for the gas analysis. The analysis could be completed within three minutes.

CHAPTER IV

MATERIALS

The materials used in this study were the catalyst, the reactants hydrogen and ethylene, and a packed bed diluent.

Catalyst

The catalyst used throughout the study was nickel on alumina. The catalyst (Girdler catalyst No. T-310, sample #10-152) and an analysis of its physical characteristics were supplied free of charge by Girdler Catalysts. According to Girdler Catalysts, the internal surface area of the catalyst was 210 m^2/gm, and its weight 10-12% Ni. Pore volume contained 0.29 cc/gm below 800Å threshold diameter and 0.27 cc/gm below 140Å threshold diameter determined by the CCl_4 adsorption technique of Benesi, Bonnar, and Lee (6).

The catalyst was received as one-eighth inch pellets and was subsequently crushed in a glass mortar and pestel. The catalyst particles were classified by screening in U. S. Standard sieves. Sample sizes varying from 8-12 mesh to 200-325 mesh were used in this study. All of the catalyst samples were taken from a single crushing and screening operation.

The nickel in the catalyst was in the unreduced form (NiO). The catalyst sample for each reaction run was packed into the reactor and

then reduced. Reduction was accomplished by passing pure hydrogen over the catalyst maintained at 700°F for twelve hours. Molten Hitec heat transfer salt was used in the reactor jacket to maintain the desired reduction temperature. After reduction the catalyst was exposed only to hydrogen and ethylene. No air was allowed to contact the catalyst because it was found that oxygen markedly deactivated it.

Hydrogen

The hydrogen was taken from commercial cylinders. Manufactured by the electrolytic process, the hydrogen was about 99.9% pure. The impurities were primarily oxygen and water. The oxygen trace was converted to water by installing a Deoxo catalytic purifier for electrolytic hydrogen in the feed stream. The water was removed by passing the gas through a Drierite drying bed.

Ethylene

Pure grade ethylene was supplied free of charge by Phillips Petroleum Company. The mole percent purity by mass spectrometer was 99.3%, with trace impurities of acetylene, carbon monoxide, water, carbon dioxide, sulfur, and oxygen. The sulfur and oxygen deactivated the catalyst and were therefore removed by a heated Model C Deoxo Purifier. The water was removed by passing the gas through a Drierite drying bed.

Packed Bed Diluent

The inert particles used to dilute the catalyst bed were Ottawa sand, which is nearly pure quartz and has almost spherical grains. The sand was classified by screening in U. S. Standard sieves.

The procedure for cleaning the sand of organic and metal

contaminants was as follows. The sand was first rinsed several times with distilled water. Then the particles were boiled in an Alconox glassware cleaning solution. After several rinsings with distilled water, the sand was boiled in dilute hydrochloric acid. The sand was then rinsed several times with distilled water, drained, and dried in an oven at 180°F.

CHAPTER V

EXPERIMENTAL PROCEDURE

The description of the experimental procedure of this study is presented in five sections: method of packing the reactor, calibration of the flowmeters, catalyst reduction, reaction run, and method of analyzing the reactant and product streams.

Packing the Reactor

As mentioned in Chapter III, the reactor was packed in a particular way in order to assure essentially isothermal conditions and to maintain the bed fixed. A schematic diagram of the reactor packing is given in Figure 3. First, three inches of 3 mm glass beads were packed into the reaction tube, after the bottom thermowell had been fixed in place. Then one inch of clean 20-30 mesh Ottawa sand was packed above the glass beads. This entrance packing served to distribute the incoming gases evenly across the tube diameter before contact was made with the catalyst. Above the initial packing was packed the catalyst diluted in 100 ml of Ottawa sand. The catalyst sample (0.1 or 0.2 grams weighed accurately to one milligram) was diluted in order to spread the reaction throughout the bed, since the exothermic heat of reaction (-32,000 cal/gm-mole) was fairly large. The diluted bed reduced the possibility of hot spots developing and allowed the heat of reaction to be carried

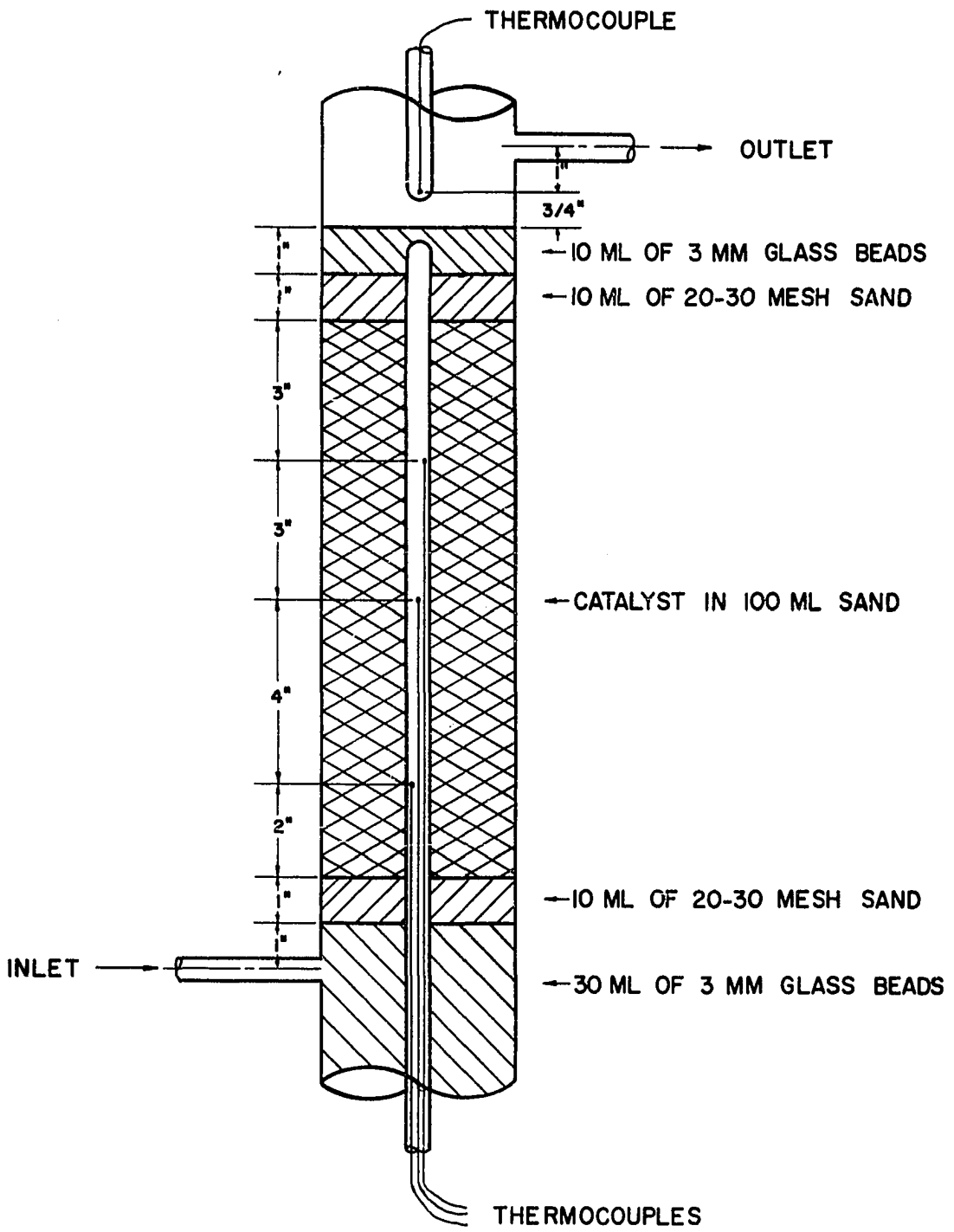

Figure 3 - Diagram of Reactor Bed Packing

off by the liquid jacket. Isothermal conditions were thus maintained throughout. During most runs the diluent Ottawa sand was 20-30 mesh, no matter what the catalyst particle size. By using the same size diluent throughout a series of runs, changes in the overall bed characteristics could be avoided. Some of these variations would be in the thermal conductivity and pressure drop of the bed. There was a limit, however, to how small a catalyst particle size could be mixed with 20-30 mesh sand. Catalyst particle sizes smaller than 100 mesh could move through the interstices of the 20-30 mesh bed. The data resulting from such a condition was erratic, especially with changes in the feed rate. Attempts were made, however, to use these particles by placing glass wool plugs at intervals through the packed bed. The purpose of these plugs was to prevent the accumulation of the small catalyst particles in the bottom or top of the reactor, or in concentrated spots. This method of packing, in order to use very small catalyst particles in a 20-30 mesh bed, was not generally successful. During some of the runs, the Ottawa sand diluent particle size was varied in order to keep it the same size as the catalyst pellets. The catalyst was diluted by rolling a weighed sample of the catalyst with the sand in a round bottom flask until a uniform mixture was observed. Above the catalyst bed was packed another one inch of clean sand and another one inch of glass beads. The reactor was cleaned and repacked for each particle size and weight of sample.

Calibration of Flowmeters

The flowmeters were calibrated before and after each run. The hydrogen and ethylene capillary manometer type flowmeters were calibrated using a rising soap-film flowmeter. In this flowmeter gas was fed into

the bottom of a calibrated tube, which contained a soap solution. The flowing gas picked up a soap film stretched across the diameter of the tube, and the gas pushed the film up the tube. By timing the volume displaced by the rising film, the volumetric flow rate was calculated. The precision of this calibration was ± 0.05 cc/sec at 10 cc/sec.

Catalyst Reduction

A weighed sample of the nickel catalyst in the unreduced form was packed into the reactor bed with the inert diluent as described earlier. The liquid jacket surrounding the reactor tube was empty at this time. Hydrogen flow at a rate of 1.176 gm-moles/hr was fed through the packed bed and was maintained throughout the reduction of the catalyst. During reaction, the hydrogen flow rate was combined with the ethylene and was varied, but was never stopped, in order to keep the reacting system free of air. After a few minutes were allowed for the hydrogen to purge the catalyst bed of air, the reactor apparatus was slowly heated. After an hour the reactor attained a temperature of 177°C. At this point 750 ml molten Hitec heat transfer salt which had previously been melted and heated to 177°C was added to the reactor jacket. The reactor and molten salt were slowly heated to 403°C, attaining this temperature after approximately four hours. Constant temperature was maintained by regulating the current flow to the heating coil surrounding the liquid jacket. The hydrogen flow had been continued during this preheating operation and continued to flow over the 403°C catalyst for eight hours.

After eight hours the Hitec molten salt was drained from the reactor, and the reactor allowed to cool slowly. After about two hours,

the reactor had cooled to room temperature.

The catalyst was completely reduced by this operation. Several test samples were analyzed for pure nickel by a procedure furnished by Girdler Catalysts (24).

Reaction Run

After the catalyst reduction operation, the liquid jacket was rinsed to remove any remaining Hitec salt, and then 1200 ml of distilled water were added. The reactor was brought up to a reacting temperature of 93°C. The reaction temperature was controlled by regulating the boiling point of the water in the reactor jacket by varying the vacuum above it. This was accomplished by regulating an air leak in the line from the vacuum pump to the air space above the boiling liquid. The boiling liquid was returned to the jacket after condensing in the liquid condenser above the reactor. In this way, total reflux was maintained and all of the liquid was returned to the boiling jacket.

After the reactor had attained the temperature of 93°C, ethylene flow was begun at 0.294 gm-moles/hr, combining it with the continuing hydrogen flow of 1.176 gm-moles/hr. This reaction mixture was continued for two hours, and then changed to a hydrogen feed of 2.350 gm-moles/hr and an ethylene feed of 0.588 gm-moles/hr for fifteen minutes. The flow was then changed to 3.528 gm-moles/hr for hydrogen, and 0.882 gm-moles/hr for ethylene for fifteen minutes. After this final feed composition, the feed rate was returned to the original rate of 1.176 gm-moles/hr for hydrogen and 0.294 gm-moles/hr for ethylene, and the reaction temperature dropped to 71°C. The same variation in feed rate was used for the 71°C run as for the 93°C run, except that each feed rate was continued for

only fifteen minutes. At this point the reaction temperature was dropped again to 40°C, and the same feed rate pattern followed.

On the basis of catalyst particle size, the Reynolds' number variations in this study ranged from 0.16 to 5.13. For a bed of 20-30 mesh particles the range in Reynolds number was from 0.64 to 1.92.

At the end of the run, the reacting conditions were returned to the original 93°C and 1.176 gm-moles/hr for hydrogen and 0.294 gm-moles/hr for ethylene feed rate. This final run was continued for fifteen minutes. All of the feed rates represented a 4:1 hydrogen to ethylene feed ratio. Product samples were analyzed every five minutes to be sure that steady state conditions had been reached.

During the reaction run the temperatures throughout the system were recorded continuously by a recording potentiometer (described in Chapter III).

Method of Analyzing the Product Stream

For the fifteen minute runs described above, samples of the product stream were analyzed at 5, 10, and 15 minutes. For the first run, two hours in duration, samples were analyzed at 5, 10, 15, 30, 60, and 120 minutes.

The gas samples of 1 cc were taken by a syringe and needle from the product stream. The reactor effluent stream and chromatograph inlet stream tubes had a rubber septum through which the gas samples were taken or injected.

During the first half and last half of a reaction run, the six standard calibration samples described previously were run through the chromatograph. They served as standards for analyzing the reactor

product stream. For an example of a calibration, see Appendix E. Since the elution curves for the ethylene-ethane system on silica gel are quite sharp, uniform and symmetrical, peak heights were used for calculating reactant conversion. Precision for conversion calculations were ± 0.5% at 20% conversion.

CHAPTER VI

EXPERIMENTAL RESULTS

The experimental results show the influence of changing the catalyst particle size at various temperatures at a given flow rate and weight of catalyst. An illustration of this influence can be seen from Figure 4, which considers reaction at a bulk temperature of 93°C. The reaction occurs entirely on the exterior surface of the catalyst particle, as will be shown later.

The reaction rate was calculated by using the basic rate equation for a catalytic flow reactor:

$$rdW = Fdx$$

or

$$r = \frac{dx}{d\left(\frac{W}{F}\right)} \simeq \frac{\Delta x}{\Delta\left(\frac{W}{F}\right)}$$

where r = rate of conversion, gm-moles converted per catalyst weight per hour

W = weight of catalyst, gm

F = feed rate to the reactor, gm-moles/hr

x = conversion, gm-moles converted/gm-mole of entering feed

The reactor was operated at differential conditions whenever possible. When the x vs. (W/F) plot was not a straight line from the origin, the slope of the curve was used to determine the reaction rate.

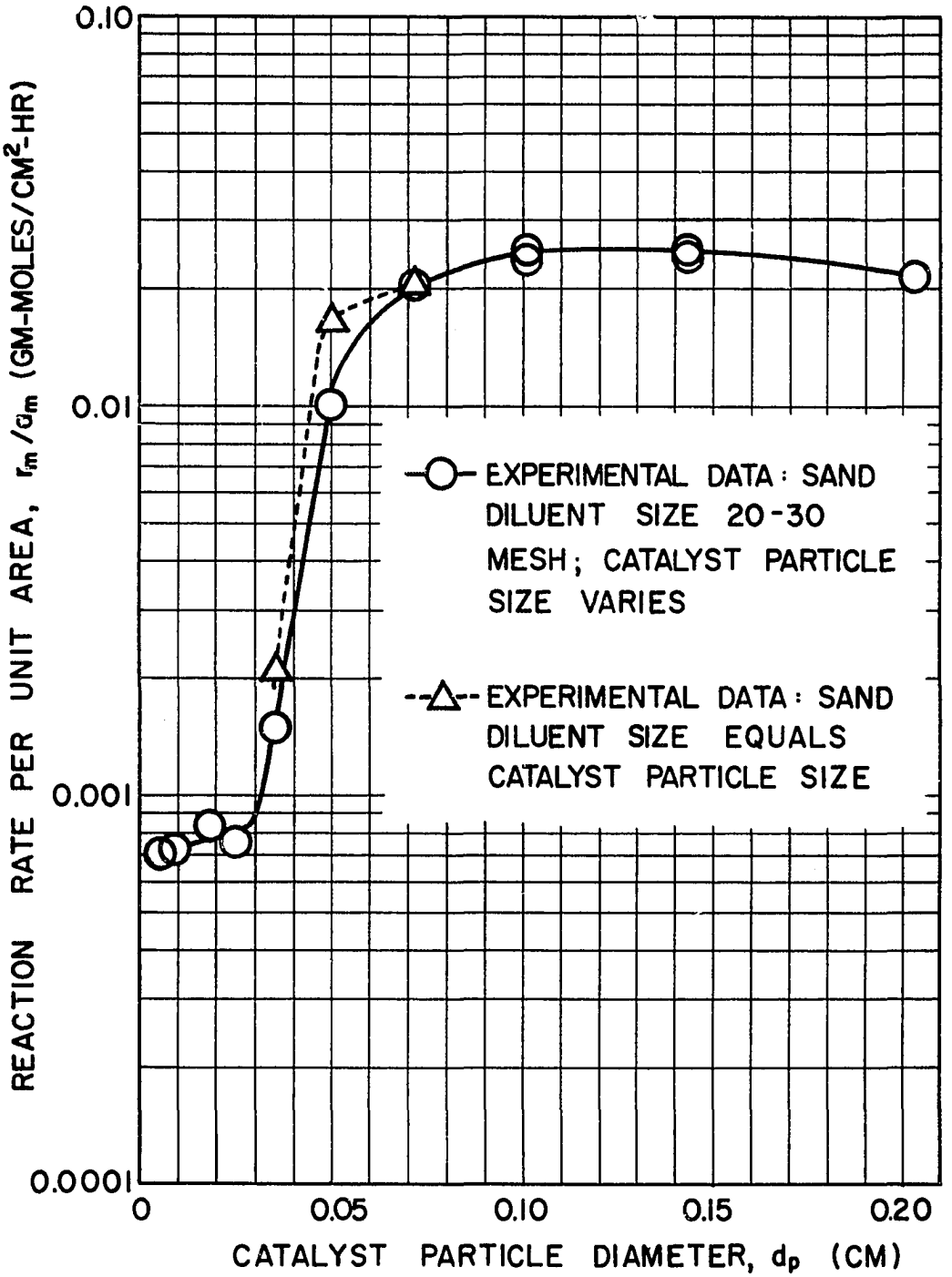

Figure 4 - Influence of Particle Size on Reaction Rate

The circles (solid line) in Figure 4 represent experimental data taken with the catalyst particles diluted in cleaned 20-30 mesh Ottawa sand. The triangles (dashed line) represent data taken with the catalyst diluted in cleaned Ottawa sand having the same particle size as the catalyst.

Beginning with the smaller particles at the left of Figure 4, an increase in particle diameter resulted in a small increase in reaction rate per unit area. At a particle diameter of about 0.03 cm the reaction rate began to rise sharply. At a particle diameter of about 0.09 cm, the reaction rate arrived at a plateau. The rate continued at this plateau for increasingly larger particle sizes, except for the largest size, where the rate dropped slightly. For a threefold increase in particle diameter of 0.03 to 0.09 cm, the reaction rate jumped approximately thirtyfold. On either side of this transition the reaction rate remained relatively constant.

Over the transition range where the rate rose sharply with increasing particle size, the sand diluent size was varied in order to equal the size of the catalyst pellet. The curve for these data (dotted line in Figure 4) was displaced slightly from but behaved in the same way as the curve describing the data using only 20-30 mesh sand as the diluent.

At the end of each reaction run the operating conditions were returned to those at the beginning, in order to check the stability of the catalyst over the period of the run. The same reaction rate was obtained at the end of the run when given the same operating conditions, demonstrating that this catalytic system was stable. Runs for 12 hours

duration failed to show a change in catalytic activity.

Runs were made in order to test the reproducibility of the data. As with all runs, these tests involved cleaning and repacking the reactor bed between runs. It was found that the conversion reproducibility error of ±1% was well within the range of the estimated maximum deviation of ±4%.

Several runs were made which varied internal surface area while maintaining external surface area constant. For this, the reaction rate using 0.2 grams of a larger pellet size was compared with the reaction rate using 0.1 gram of a smaller pellet size, the smaller pellet having an external surface area per gram which was twice that of the larger pellet. The two samples with the equal external surface areas were found to have equal reaction rates, although their internal surface areas were different by a factor of two.

CHAPTER VII

DISCUSSION OF RESULTS

Observing the behavior of the curve of Figure 4 leads one to the conclusion that a major shift in reaction behavior occurs when the catalyst particle size is increased from 50-70 mesh to 20-30 mesh. All bulk conditions other than catalyst particle size remained constant and yet the reaction rate increased thirtyfold when the average particle size was increased from 0.03 cm to 0.09 cm. This experimental demonstration that varying the catalyst particle size has a pronounced effect on the reaction rate leads us to seek the cause of this behavior and to attempt to evaluate quantitatively and to elucidate the process.

In the previous section, it was shown that the catalyst behaved in the same manner in this transition range whether or not it was diluted with a diluent of the same particle size. That is, the reaction rate shift could not be ascribed to a caging or shielding effect on the catalyst particle by the diluent. Also, by packing the catalyst in a diluent of equal size, there could be no movement or fluidization of the catalyst particles.

Furthermore, the experiments with varying volumes of catalyst having the same surface area show that the reaction rate depended upon external surface area only. Calculations using the equations developed by Prater (45) and Schilson (36), and data examined by Ramaswami (46),

Pauls, Comings, and Smith (42), and Weisz and Hicks (60) for systems similar to the one used in this study rule out significant temperature and concentration gradients within the pellet.

Radiant heat transfer for the system used in this study would not be significant. The Ottawa sand diluent and nickel-on-alumina catalyst would transfer negligible radiant heat at the temperatures encountered, as shown by Chen and Churchill (11).

The catalyst behavior can be explained by gas-film heat and mass transfer correlations for the behavior of particles in a packed bed. These transport phenomena are introduced in terms of the j-factor correlations. The purpose of these j-factor correlations is to obtain heat and mass transfer coefficients which can be used to determine the partial pressure and temperature gradients in the gas film surrounding the catalyst pellet. In the case of mass transfer, the correlations may be used as follows:

$$r_{m_i} = k_{G_i} a_m \varnothing (p_{i_S} - p_{i_B})$$

or

$$(p_{i_S} - p_{i_B}) = \Delta p_i = \frac{r_{m_i}}{a_m \varnothing k_{G_i}} \qquad \text{(VII-1)}$$

where r_{m_i} = rate of reaction per unit weight of catalyst for component i, gm-moles/hr gm

a_m = surface area of the pellets per unit weight of the catalyst, cm^2/gm

p_{i_S} = partial pressure of component i at the catalyst surface, atm

p_{i_B} = partial pressure of component i in the bulk gas phase, atm

Solving Equation (II-2) for $1/k_{G_i}$

$$\frac{1}{k_{G_i}} = \frac{P_f}{G_M} (j_D)^{-1} \left(\frac{\mu}{\rho_g D_i} \right)_f^{2/3} \qquad \text{(VII-2)}$$

Substituting Equation (VII-2) into Equation (VII-1),

$$P_{i_S} - P_{i_B} = \frac{r_{m_i} P_f}{a_m \phi G_M} (j_D)^{-1} \left(\frac{\mu}{\rho_g D_i} \right)_f^{2/3} \qquad \text{(VII-3)}$$

In a similar manner the expression for the temperature gradient across the film may be derived. The heat generation is equal to heat release at steady state:

$$r_{m_i} \Delta H_i = h_G a_m \phi (T_S - T_B)$$

or

$$(T_S - T_B) = \Delta T = \frac{r_{m_i} \Delta H_i}{a_m \phi h_G} \qquad \text{(VII-4)}$$

where T_S = temperature at the catalyst surface, ^{o}K

T_B = temperature of the bulk gas, ^{o}K

ΔH_i = heat of reaction for component i, cal/gm-mole

Solving Equation (II-1) for $1/h_G$

$$\frac{1}{h_G} = \frac{1}{C_{p_M} G_M} (j_H)^{-1} \left(\frac{C_{p_m} \mu}{k} \right)_f^{2/3} \qquad \text{(VII-5)}$$

Substituting Equation (VII-5) into (VII-4),

$$T_S - T_B = \frac{r_{m_i} \Delta H_i}{a_m \phi C_{p_M} G_M} (j_H)^{-1} \left(\frac{C_{p_m} \mu}{k} \right)_f^{2/3} \qquad \text{(VII-6)}$$

In order to use Equations (VII-3) and (VII-6) to determine the partial pressure and temperature gradients across the gas film surrounding the catalyst particle, it is necessary to have suitable j-factor correlations for mass and heat transfer. The heat transfer correlation of Denton (16) was judged the most appropriate for this study for several

reasons. First, his data was taken with only a gas film surrounding the pellet and did not introduce the added complexity of a gas-liquid film. As discussed in Chapter II, the correlations with only a gas film involved are more appropriate to a gas phase heterogeneous reaction.

Second, Denton's values for the j-factor correlation with Reynolds number is in line with the majority of the other gas film correlations.

Third, and most important, Denton's data was taken in a system similar to the one used in this study. He measured the steady state heat transfer coefficients by generating heat in a single metal sphere randomly packed in a bed of glass spheres. A similar situation exists in the reactor bed used in this study. The catalyst pellet, which generates the heat, is randomly packed in a bed of relatively spherical sand grains. The catalyst pellets are essentially isolated from each other because the volumetric ratio of the reactor bed packing is approximately 1:100 = catalyst:sand. The similarity of the two systems tends to eliminate the problem of variables specific to the particular system in question. For example, the magnitude of pellet-to-pellet heat conduction through the solid point contacts cannot be assessed. There has been some recent work on the problem of point-to-point heat transfer (37) in a packed bed, but actual calculation of the magnitude of this phenomena is not as yet possible. The situation is further complicated when only one particle among many is generating heat, which was the case in this study. Denton's correlation, however, includes this effect, and calculation of surface temperatures for a particle generating heat among inert particles should be more accurate using his correlation.

The relationship between heat and mass transfer j-factors for a reacting system is found in the research of Satterfield and Resnick (50). They decomposed hydrogen peroxide in a bed of metal spheres, measuring both the heat and mass transfer characteristics of the system. They found the ratio $j_H/j_D = 1.37$.

Utilizing the heat and mass transfer studies of Denton (16) and Satterfield and Resnick (50), one obtains the correlations:

$$j_H = 0.584(Re)^{-0.30} \qquad \text{(VII-7)}$$

$$j_D = 0.426(Re)^{-0.30} \qquad \text{(VII-8)}$$

Substituting Equation (VII-8) into Equation (VII-3), the partial pressure gradient of a component across the gas film may be calculated:

$$p_{i_S} - p_{i_B} = \Delta p_i = \frac{r_m}{a_m} \cdot \frac{P_f}{G_M \phi} \cdot \frac{1}{(0.426)} \left(\frac{d_p G_m}{\mu}\right)^{0.30} \left(\frac{\mu}{\rho_g D_i}\right)_f^{2/3}$$

$$= \frac{r_m}{a_m} d_p^{0.30} \left[\frac{P_f}{G_M \phi} \cdot \frac{1}{(0.426)} \left(\frac{G_m}{\mu}\right)^{0.30} \left(\frac{\mu}{\rho_g D_i}\right)_f^{2/3} \right]$$

$$= \gamma \frac{r_m}{a_m} d_p^{0.30} \qquad \text{(VII-9)}$$

where $\gamma = \left[\frac{P_f}{G_M \phi} \cdot \frac{1}{(0.426)} \left(\frac{G_m}{\mu}\right)^{0.30} \left(\frac{\mu}{\rho_g D_i}\right)_f^{2/3} \right]$ (VII-10)

The temperature change from the bulk gas stream to the external surface of the catalyst may be calculated from Equations (VII-6) and (VII-7):

$$T_B - T_S = \Delta T = \frac{r_m}{a_m} \cdot \frac{\Delta H}{\phi C_{p_M} G_M} \cdot \frac{1}{(0.584)} \cdot \left(\frac{d_p G_m}{\mu}\right)^{0.30} \left(\frac{C_p \mu}{k}\right)_f^{2/3}$$

$$= \frac{r_m}{a_m} d_p^{0.30} \left[\frac{\Delta H}{\phi C_{p_M} G_M} \cdot \frac{1}{(0.584)} \left(\frac{G_m}{\mu} \right)^{0.30} \left(\frac{C_{p_m} \mu}{k} \right)_f^{2/3} \right]$$

$$= \beta \frac{r_m}{a_m} d_p^{0.30} \qquad \text{(VII-11)}$$

where $$\beta = \left[\frac{\Delta H}{\phi C_{p_M} G_M} \cdot \frac{1}{(0.584)} \left(\frac{G_m}{\mu} \right)^{0.30} \left(\frac{C_{p_m} \mu}{k} \right)_f^{2/3} \right] \qquad \text{(VII-12)}$$

The terms β and γ are functions of temperature and were calculated from physical and transport properties available in the literature. The arithmetic average gas film temperature was used for the physical properties of the gases. Sample calculations for the influence of temperature on β and γ are given in Appendix C. Using the smoothed experimental values (see Appendix B) for r_m/a_m and d_p, the values of partial pressures at the catalyst surface for various particle sizes were calculated from the measured values of the rate. The calculation of Δp and ΔT were accomplished by a trial and error solution of the following four simultaneous equations:

$$\Delta P = \gamma \frac{r_m}{a_m} d_p^{0.30} \qquad \text{(VII-9)}$$

$$\Delta T = \beta \frac{r_m}{a_m} d_p^{0.30} \qquad \text{(VII-11)}$$

$$\beta = f_1(T) \qquad \text{(VII-12)}$$

$$\gamma = f_2(T) \qquad \text{(VII-10)}$$

Examples of the values of surface temperatures and concentrations are shown in Figure 5. Studying Figure 5 from left to right, one

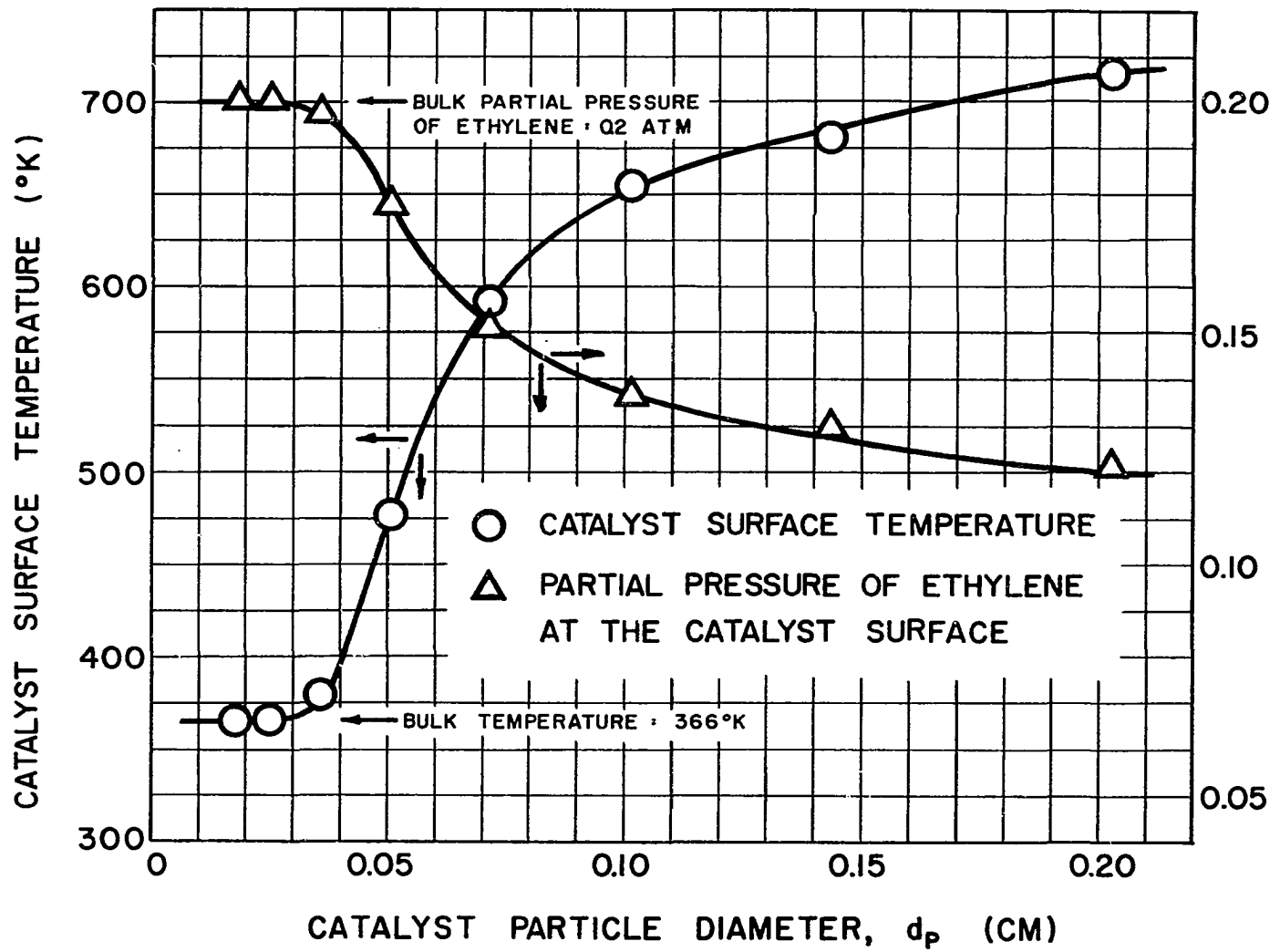

Figure 5 - Catalyst Surface Partial Pressure and Temperature as a Function of Particle Diameter

sees that the temperature at the surface of the catalyst particle generally increases with increasing particle diameter. At first, however, the smaller particles show only a slight change in surface temperature with increasing particle size. At the 0.03 cm particle size the temperature begins to rise abruptly. As the particle size increases, the temperature continues to increase and finally begins to taper off at the larger particle sizes.

The partial pressures of ethylene at the surface of the catalyst behaves inversely from that of the surface temperature. As the particle size increases the partial pressure of ethylene at the surface decreases.

Using these calculated values of surface temperatures and concentrations, an Arrhenius type function of log r vs. 1/T was plotted in Figure 6. A sample calculation of these points is given in Appendix D. From Figure 6 the energies of activation and frequency factors for the reaction levels can be calculated. For the small particles (lower reaction level) the Arrhenius energy of activation is 9.6 kcal/gm-mole and the frequency factor is 2,900 gm-moles/hr cm^2 atm^2. For the larger particles (upper reaction plateau) the energy of activation is 1.96 kcal/gm-mole and the frequency factor is 1.18 gm-moles/hr cm^2 atm^2.

The energy of activation for the small particles, 9.6 kcal/gm-mole, is somewhat lower than Beeck's (5) value of 10.7 kcal/gm-mole. The value of 9.6 kcal/gm-mole is, however, close enough to Beeck's value to insure that the chemical reaction kinetics is primarily the rate controlling step. The calculated catalyst surface temperatures for the small particles (50-70 and 70-100 mesh) in this study find the surface

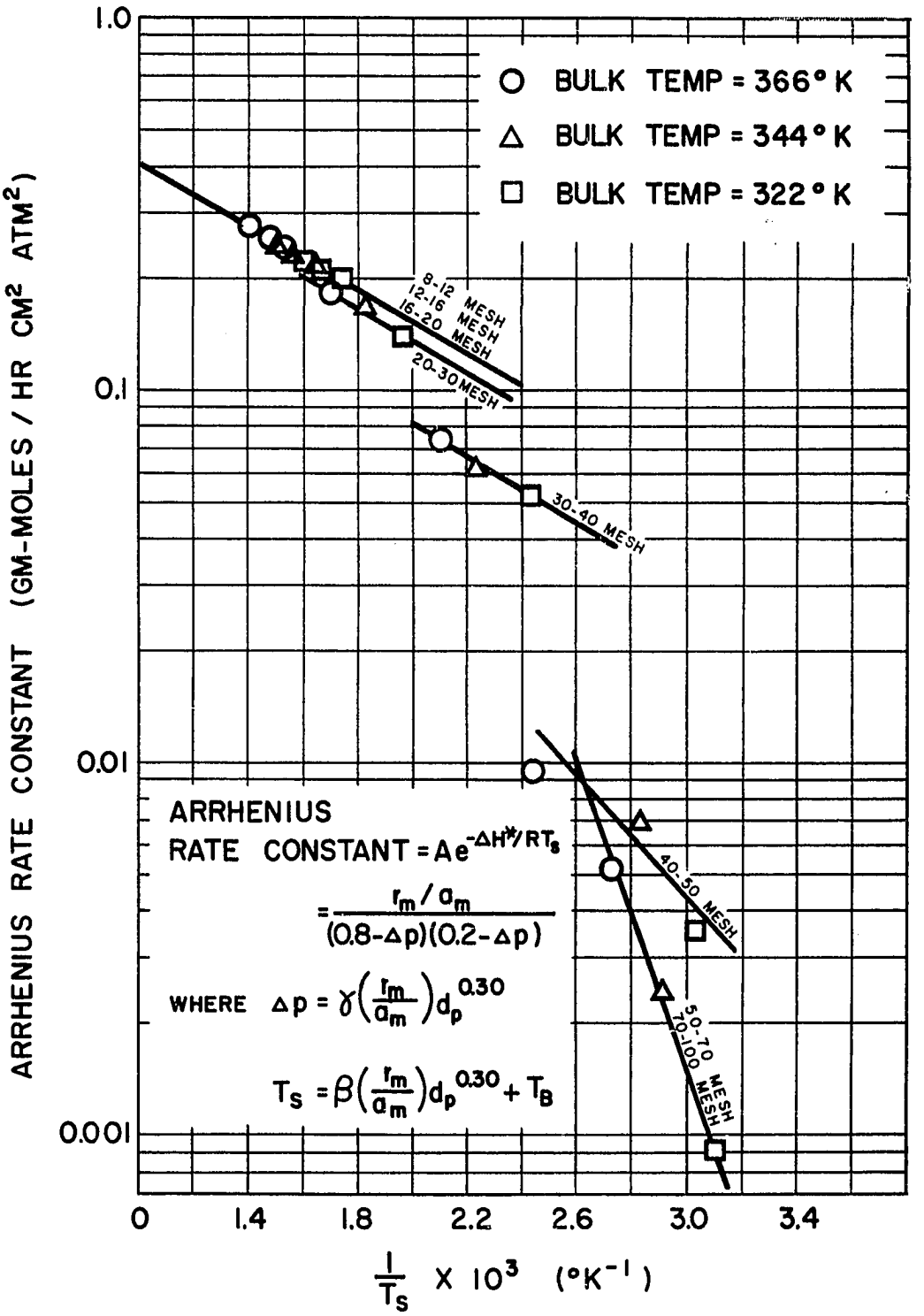

Figure 6 - Arrhenius Plot for Activation Energy and Frequency Factor

temperatures essentially the same as the bulk gas temperatures, 40°C, 71°C, and 93°C. These surface temperatures are within the range of Beeck's study. If the reaction were diffusion controlled, the rate would be considerably lower than the 9.6 kcal/gm-mole value.

The energy of activation for the increasingly larger particles decreases and then levels out at a value of 1.96 kcal/gm-mole. The calculated surface temperatures for the larger catalyst pellets (8-12, 12-16, and 16-20 mesh) show that they have considerably higher surface temperatures than the smaller pellets, ranging from 381 to 443°C. The literature reports that for temperatures above 150 to 200°C the energy of activation decreases. The reports differ on the energy of activation found, and there seems to be no agreement on what should be a reasonable value. However, most of these studies do agree that the energy of activation above 150 to 200°C should be below 3.4 kcal/gm-mole. Therefore, the energy of activation of 1.96 kcal/gm-mole found in this study seems reasonable, although possibly somewhat low. The value of 1.96 kcal/gm-mole was evaluated using the calculated surface temperatures and partial pressures and is considerably lower than Beeck's 10.7 kcal/gm-mole. Thus the drop in activation energy must result from a change in the reaction mechanism rather than from a diffusion controlling condition.

Also, the decrease in equilibrium constant with increasing temperature does not become a limiting factor. A surface temperature of about 1000°K would be required before the reversible reaction would become significant. The equilibrium constant for the hydrogenation of ethylene is 3.2×10^{17} at 300°K, 3.2×10^{3} at 716°K (the highest calculated surface temperature), and 0.35 at 1000°K.

What happened in this reaction process was that a sharp rise in catalyst surface temperature with increasing particle size shifted the chemical reaction mechanism or chemical reaction rate controlling step. This new mechanism, in turn, operated at a high reaction temperature and high reaction rate. As a result, the catalyst interface became depleted in ethylene, and the molecular diffusion to the surface became the slowest step in the overall process. This depleted condition can best be seen from Figure 5. For the larger particles the surface temperature was high but the partial pressure of reactant at the interface was low. The overall reaction became diffusion controlled in the upper thermal regime.

A more graphic description of this reaction process can be given by plotting the reaction rates for the two mechanisms, using the calculated catalyst surface temperatures and partial pressures, and the evaluated Arrhenius energies of activation and frequency factors. The reaction rates can be calculated using the following equations:

Literature rate equation: $$\left(\frac{r_m}{a_m}\right) = A p_{H_2} p_{C_2H_4} e^{-\Delta H^*/RT_s}$$

For small particles: $$\left(\frac{r_m}{a_m}\right)_1 = 2{,}900\ (0.8 - \Delta p)(0.2 - \Delta p) e^{-9{,}600/RT_s}$$

For large particles: $$\left(\frac{r_m}{a_m}\right)_2 = 1.18\ (0.8 - \Delta p)(0.2 - \Delta p) e^{-1{,}960/RT_s}$$

The experimentally evaluated data were substituted into these two rate equations and the resulting reaction rates were plotted in Figure 7.

Beginning at the lower left of Figure 7, one can see that the first reaction rate (for small particles) began to rise at a catalyst particle diameter of 0.03 cm. The rate increased sharply, rising over

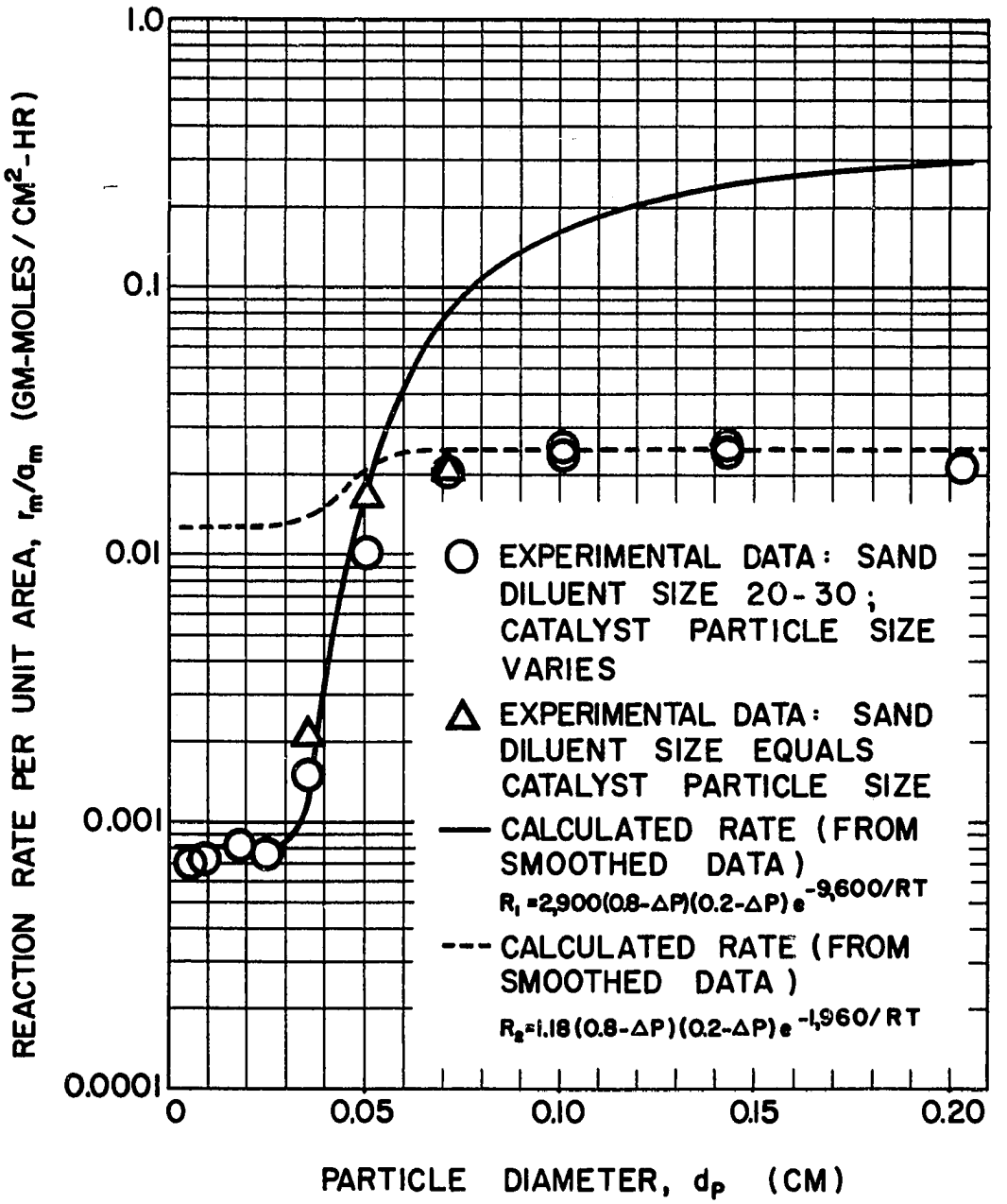

Figure 7 - Reaction Rate from Proposed Rate Equations as a Function of Particle Diameter

two orders of magnitude before it began to level off. During this rise, which could only be due to an exponential rise in temperature, the temperature increase at the catalyst surface caused a shift in the chemical reaction mechanism. As a result, the mechanism shifted to the second rate expression, shown by the dashed line in Figure 7. This second reaction rate became controlled by the diffusion step and leveled off in line with the experimental data points. Therefore, two shifts occurred during the transition phase, both of them resulting from an increase in surface temperature due to an increase in catalyst particle size. First, the increase in temperature induced a change in reaction mechanism. This mechanism change has been documented in the literature and discussed in Chapter II. Second, the increase in temperature shifted the rate controlling step from reaction kinetics controlling in the lower thermal regime to film diffusion controlling in the upper thermal regime. This second shift was the cause of the levelling off of the experimental reaction rates for the larger particles, and was also the reason calculated values for the second reaction rate expression level off along with the experimental values. This shift from reaction kinetics to diffusion controlling steps was explained by Frank-Kamenetskii, as shown in Chapter II and Appendix A.

CHAPTER VIII

CONCLUSIONS

Catalyst particle size may exert a strong influence upon the observed reaction rate for an exothermic surface reaction in a packed bed flow reactor. This marked change in reaction rate is consistent with the theory of surface thermal regimes developed by Frank-Kamenetskii. Increasing the catalyst particle size shifts the reaction from chemical reaction kinetics controlling (lower thermal regime) to gas film controlling (upper thermal regime).

The j-factor correlations for gas film systems adequately evaluate changes in catalyst surface temperatures and concentrations, and these calculated changes are consistent with experimental results and literature values. Furthermore, the j-factor correlations are satisfactorily employed with a diluted catalyst bed, and the inert diluent particles may be either larger than, equal to, or smaller than the catalyst particles.

NOMENCLATURE

a_m = external surface area of the catalyst particles per unit weight, cm^2/gm

a_p = surface area of an individual particle, cm^2/particle

a_v = surface area of catalyst particles per unit volume of the bed, cm^2/cm^3

A = Arrhenius frequency factor, gm-moles/hr cm^2 atm^2

A_{cs} = cross sectional area of the bed, cm^2

C_{p_m} = heat capacity per unit mass at constant pressure, cal/gm ^oK

C_{p_M} = molal heat capacity at constant pressure, cal/gm-mole ^oK

d_p = average catalyst particle diameter, cm

D_i = gas phase diffusion coefficient of component i, cm^2/sec

D_t = diameter of packed column, cm

$f(\ )$ = mathematical function

F = feed rate to the reactor, gm-moles/hr

G_m = superficial mass velocity of the gas based upon the total cross sectional area of the bed, gm/cm^2 hr

G_M = superficial molal velocity of the gas based upon the total cross sectional area of the bed, gm-moles/cm^2 hr

h_G = gas phase heat transfer coefficient, cal/cm^2 hr ^oK

j_D = mass transfer number, dimensionless

j_H = heat transfer number, dimensionless

k = gas thermal conductivity, cal/cm^2 hr ^oK

k = reaction rate constant, gm-moles/hr cm^2 atm^2

k_G = gas phase mass transfer coefficient, gm-moles/cm^2 hr

p = partial pressure, atm

p_f = pressure factor, defined as the logarithmic mean value of the partial pressure over the boundary limits of the gas film, atm

Pr = Prandtl number, $\left(\frac{C_{p_m}\mu}{k}\right)$, dimensionless

r_m = rate of reaction per unit weight of catalyst, gm-moles/hr gm

Re = Reynolds number, $\left(\frac{d_p G_m}{\mu}\right)$, dimensionless

Sc = Schmidt number, $\left(\frac{\mu}{\rho_g D_i}\right)$, dimensionless

T = temperature, ^oK

W = weight of catalyst, gm

x = conversion, gm-moles converted per gram mole of entering feed

y = mole fraction

β = heat transfer group (see Equation VII-12), $^oK\ cm^2\ hr\ cm^{-0.3}\ gm\text{-}mole^{-1}$

γ = mass transfer group (see Equation VII-10), $atm\ cm^2\ hr\ cm^{-0.3}\ gm\text{-}mole^{-1}$

ΔH = heat of reaction, cal/gm-mole

ΔH^* = Arrhenius energy of activation, cal/gm-mole

ϵ = bed void fraction

$\frac{\epsilon}{k}$ = Lennard-Jones force constant/Boltzmann's constant

μ = gas viscosity, poise or gm/cm sec

π = total pressure, atm

ρ_g = average density of the gas phase, gm/cm^3

σ = Lennard-Jones force constant

ϕ = particle shape factor as defined by Gamson (22), equal to the ratio of actual external surface area available for mass transfer to the total external surface area, dimensionless

Ω_D = collision integral

Subscripts

B = bulk gas phase

c = critical value

f = average film characteristic

i = component i

m = mass basis

M = mole basis

mv = mean value

P = Product

r = reduced value

R = reactant

S = catalyst surface

1, 2 = reaction 1 and 2, or component 1 and 2

Superscript

Primes refer to pseudo-values in viscosity calculation

LITERATURE CITED

1. American Institute of Chemical Engineers, "Dynamic Objectives for Chemical Engineering," Chem. Eng. Progr., 57, 81 (1961).

2. Aris, R., "On Shape Factors for Irregular Particles," Chem. Eng. Science, 6, 262 (1957).

3. Bar-Ilan, M. and Resnick, W., "Gas-Phase Mass Transfer in Fixed Beds at Low Reynolds Numbers," Ind. and Eng. Chem., 49, 313 (1957).

4. Baumister, E. B. and Bennett, "Fluid-particle Heat Transfer in Packed Beds," A.I.Ch.E. J., 4, 69 (1958).

5. Beeck, O., "Hydrogenation Catalysts," Disc. Faraday Soc., 8, 118 (1950).

6. Benesi, H. A., Bonner, R. U., and Lee, C. F., "Determination of Pore Volume of Solid Catalysts," Anal. Chem., 27, 1963 (1955).

7. Bond, G. C., Catalysis by Metals, Academic Press, New York, 1962.

8. Bradshaw, R. D. and Bennett, C. O., "Fluid-particle Mass Transfer in a Packed Bed," A.I.Ch.E. J., 7, 48 (1961).

9. Carberry, J. J., "A Boundary-Layer Model of Fluid-Particle Mass Transfer in Fixed Beds," A.I.Ch.E. J., 6, 460 (1960).

10. Carberry, J. J., "The Catalytic Effectiveness Factor Under Nonisothermal Conditions," A.I.Ch.E. J., 7, 350 (1961).

11. Chen, J. C. and Churchill, S. W., "Radiant Heat Transfer in Packed Beds," A.I.Ch.E. J., 9, 35 (1963).

12. Chilton, T. H. and Colburn, A. P., "Mass Transfer (Absorption) Coefficients," Ind. Eng. Chem., 26, 1183 (1934).

13. Chu, C. and Hougen, O. A., "The Effect of Adsorption on the Effectiveness Factor of Catalyst Pellets," Chem. Eng. Sci., 17, 167 (1962).

14. Chu, J. C., Kalil, J., and Wetteroth, W. A., "Mass Transfer in a Fluidized Bed," Chem. Eng. Progr., 49, 141 (1953).

15. Crawford, E., Roberts, M. W., and Kemball, C., "Hydrogenation of

Ethylene on Sintered Nickel Films," Trans. Faraday Soc., 58, 1761 (1962).

16. Denton, W. H., Inst. Mech. Engrs. and Am. Soc. Mech. Engrs.' Proc. General Discussion of Heat Transfer, pp. 370-386, Inst. Mech. Engrs., London, England, 1951.

17. Eley, D. D., Catalysis, Vol. 3, p. 49, Reinhold, New York, 1955.

18. Eyring, H., Colburn, C. B., and Zwolinski, B. J., "The Activated Complex in Chemisorption and Catalysis," Disc. Faraday Soc., 8 39 (1950).

19. Eichhorn, J. and White, R. R., "Particle-to-Fluid Heat Transfer in Fixed and Fluidized Beds," Chem. Eng. Progr. Symposium Series, 4, 11 (1951).

20. Foss, T. G. and Eyring, H., "Catalytic Hydrogenation of Ethylene over Evaporated Nickel," J. Phys. Chem., 62, 103 (1958).

21. Frank-Kamenetskii, D. A., Diffusion and Heat Exchange in Chemical Kinetics, Princeton University Press, Princeton, N. J., 1955.

22. Gamson, B. W., "Heat and Mass Transfer," Chem. Eng. Progr., 47, 19 (1951).

23. Gamson, B. W., Thodos, G., and Hougen, O. A., "Heat, Mass and Momentum Transfer in the Flow of Gases Through Granular Solids," Trans. A.I.Ch.E., 39, 1 (1943).

24. Girdler Catalysts, "Modified Procedure for the Determination of Reduced Nickel in G-15," Girdler SM-C-8f, 1952.

25. Glaser, M. B. and Thodos, G., "Heat and Momentum Transfer in the Flow of Gases Through Packed Beds," A.I.Ch.E. J., 4, 63 (1958).

26. Hirschfelder, J. O., Curtiss, C. F., and Bird, R. B., Molecular Theory of Gases and Liquids, Wiley, New York, 1954.

27. Hoelscher, H. E., Poynter, W. G., and Weger, E., "The Vapor-Phase Hydrogenation of Olefins," Chem. Rev., 54, 575 (1954).

28. Hoelscher, H. E., "A Reactor Design Equation Based on a Proposed Distributed Boundary-Layer Thickness," A.I.Ch.E. J., 4, 300 (1958).

29. Hougen, O. A., "Engineering Aspects of Solid Catalysts," Ind. Eng. Chem., 53, 509 (1961).

30. Hougen, O. A., Watson, K. M., and Ragatz, R. A., Chemical Process Principles. Part I, 2nd ed., Wiley, New York, 1956.

31. Hougen, O. A., Watson, K. M., Chemical Process Principles. Part III,

Wiley, New York, 1957.

32. Hurt, D. M., "Principles of Reactor Design: Gas-Solid Interface Reactions," Ind. Eng. Chem., 35, 522 (1943).

33. Jenkins, G. I. and Rideal, E., "The Catalytic Hydrogenation of Ethylene at a Nickel Surface. Part 1. The Chemisorption of Ethylene," J. Chem. Soc. (London), 158, 2490 (1955).

34. Jenkins, G. I. and Rideal, E., "The Catalytic Hydrogenation of Ethylene at a Nickel Surface. Part II. The Reaction Mechanism," J. Chem. Soc. (London), 158, 2496 (1955).

35. Kusik, C. L. and Happel, J., "Boundary-Layer Mass Transport with Heterogeneous Catalysis," Ind. Eng. Chem. Fundamentals, 1, 163 (1962).

36. Laidler, K. J. and Townshend, R. E., "Kinetics of Hydrogenation of Ethylene on Evaporated Nickel and Iron Films," Trans. Faraday Soc., 57, 1590 (1961).

37. Masamune, S. and Smith, J. M., "Thermal Conductivity of Beds of Spherical Particles," Ind. Eng. Chem. Fundamentals, 2, 136 (1963).

38. Mingle, J. O. and Smith, J. M., "Effectiveness Factors for Porous Catalysts," A.I.Ch.E. J., 7, 243 (1961).

39. McCune, L. K. and Wilhelm, R. H., "Mass and Momentum Transfer in Solid-Liquid System," Fixed and Fluidized Beds," Ind. Eng. Chem., 41, 1124 (1949).

40. Norris, T., "Vapor Phase Chromatography Apparatus," M.S. Thesis, Univ. of Oklahoma, Norman, Okla., 1957.

41. Park, W. H., "Study on Packed Bed--Its Analytical Description and Solution," Ph.D. Thesis, Univ. of Minnesota, Minneapolis, Minn., 1960.

42. Pauls, A. C., Comings, E. W., and Smith, J. M., "Kinetics of the Hydrogenation of Ethylene," A.I.Ch.E. J., 5, 453 (1959).

43. Perry, J. H., ed., Chemical Engineers' Handbook, 3rd ed., McGraw-Hill, New York, 1950.

44. Pfeffer, R. and Happel, J., "An Analytical Study of Heat and Mass Transfer in Multiparticle Systems at Low Reynolds Numbers," paper delivered during the A.I.Ch.E. Fiftieth National Meeting, Buffalo, New York, May 1963.

45. Prater, C. D., "The Temperature Produced by Heat of Reaction in the Interior of Porous Particles," Chem. Eng. Sci., 8, 284 (1958).

46. Ramaswami, D., "Reaction Rates in Fluid Systems Catalyzed by Solid Particles in Fixed Beds," Ph.D. Thesis, Univ. of Wisconsin, Madison, Wis., 1961.

47. Reid, R. C. and Sherwood, T. K., The Properties of Gases and Liquids, McGraw-Hill, New York, 1958.

48. Resnick, W. and White, R. R., "Mass Transfer in Systems of Gas and Fluidized Solids," Chem. Eng. Progr., 45, 377 (1949).

49. Rosner, D. E., "The Apparent Chemical Kinetics of Surface Reactions in External Flow Systems: Diffusional Falsification of Activation Energy and Reaction Order," A.I.Ch.E. J., 9, 321 (1963).

50. Satterfield, C. N. and Resnick, H., "Simultaneous Heat and Mass Transfer in a Diffusion Controlled Chemical Reaction," Chem. Eng. Progr., 50, 504 (1954).

51. Schilson, R. E., "Study of Intraparticle Diffusion Effects in a Gas Phase Catalytic Reaction," Ph.D. Thesis, Univ. of Minnesota, Minneapolis, Minn., 1958.

52. Schilson, R. E. and Amundson, N. R., "Intraparticle Diffusion and Conduction in Porous Catalysts. I. Single Reactions," Chem. Eng. Sci., 13, 226 (1961).

53. Schilson, R. E. and Amundson, N. R., "Intraparticle Diffusion and Conduction in Porous Catalysts. II. Complex Reactions," Chem. Eng. Sci., 13, 237 (1961).

54. Skinner, J. L., "Kinetic Study of the Formation of Cyclohexene from Ethylene and Butadiene at Elevated Pressures and Temperatures," Ph.D. Thesis, Univ. of Oklahoma, Norman, Okla., 1962.

55. Smith, J. M., Chemical Engineering Kinetics, McGraw-Hill, New York, 1956.

56. Thiele, E. W., "Relation Between Catalytic Activity and Size of Particle," Ind. Eng. Chem., 31, 916 (1939).

57. Tinkler, J. D. and Metzner, A. B., "Reaction Rates in Nonisothermal Catalysts," Ind. Eng. Chem., 53, 663 (1961).

58. Twigg, G. H., "The Mechanism of the Catalytic Hydrogenation of Ethylene," Disc. Faraday Soc., 8, 152 (1950).

59. von Rosenberg, D. U., Durrill, P. L., and Spencer, E. H., "Numerical Solution of Partial Differential Equations Representing Fixed Bed Reactions," Brit. Chem. Eng., 320 (March 1962).

60. Weisz, P. B. and Hicks, J. S., "The Behavior of Porous Catalyst

Particles in View of Internal Mass and Heat Diffusion Effects," Chem. Eng. Sci., 17, 265 (1962).

61. Wheeler, A., "Reaction Rates and Selectivity in Catalyst Pores," Advances in Catalysis, III, p. 249, Academic Press, New York, 1951.

62. Wilkie, C. R. and Hougen, O. A., "Mass Transfer in the Flow of Gases Through Granular Solids Extended to Low Modified Reynolds Numbers," Trans. A.I.Ch.E., 41, 445 (1945).

APPENDIX A

THERMAL REGIMES OF THE CATALYST SURFACE

APPENDIX A

THERMAL REGIMES OF THE CATALYST SURFACE

The thermal regimes of the catalyst surface were explained by Frank-Kamenetskii, and the experimental verifications of his theory are reviewed in his book (21). His ideas are presented in Figure 8.

Curve G1 represents the rate of reaction, or the heat generated per unit surface area per unit time. The left hand portion of the curve corresponds to the reaction kinetics range, where the rate of reaction increases exponentially with temperature and is independent of flow velocity. The right hand portion of the curve corresponds to the diffusional range, where the overall rate of reaction is a weak function of temperature but is a strong function of flow velocity. Curves G2 and G3 represent greater and smaller flow velocities, respectively. Curves R1 through R5 represent the intensity of heat removal from the surface under various conditions, expressed in the same units.

The thermal regime of the surface depends upon the mutual position of the heat generation (G) curves and the heat removal (R) curves. The points of intersection for different positions of the curves determine the stationary state at the surface. It is assumed that the gas at the surface and the catalyst surface are at the same temperature.

For heat removal curve R1 and heat generation curve G1, the only stationary state possible is point n, corresponding to a small

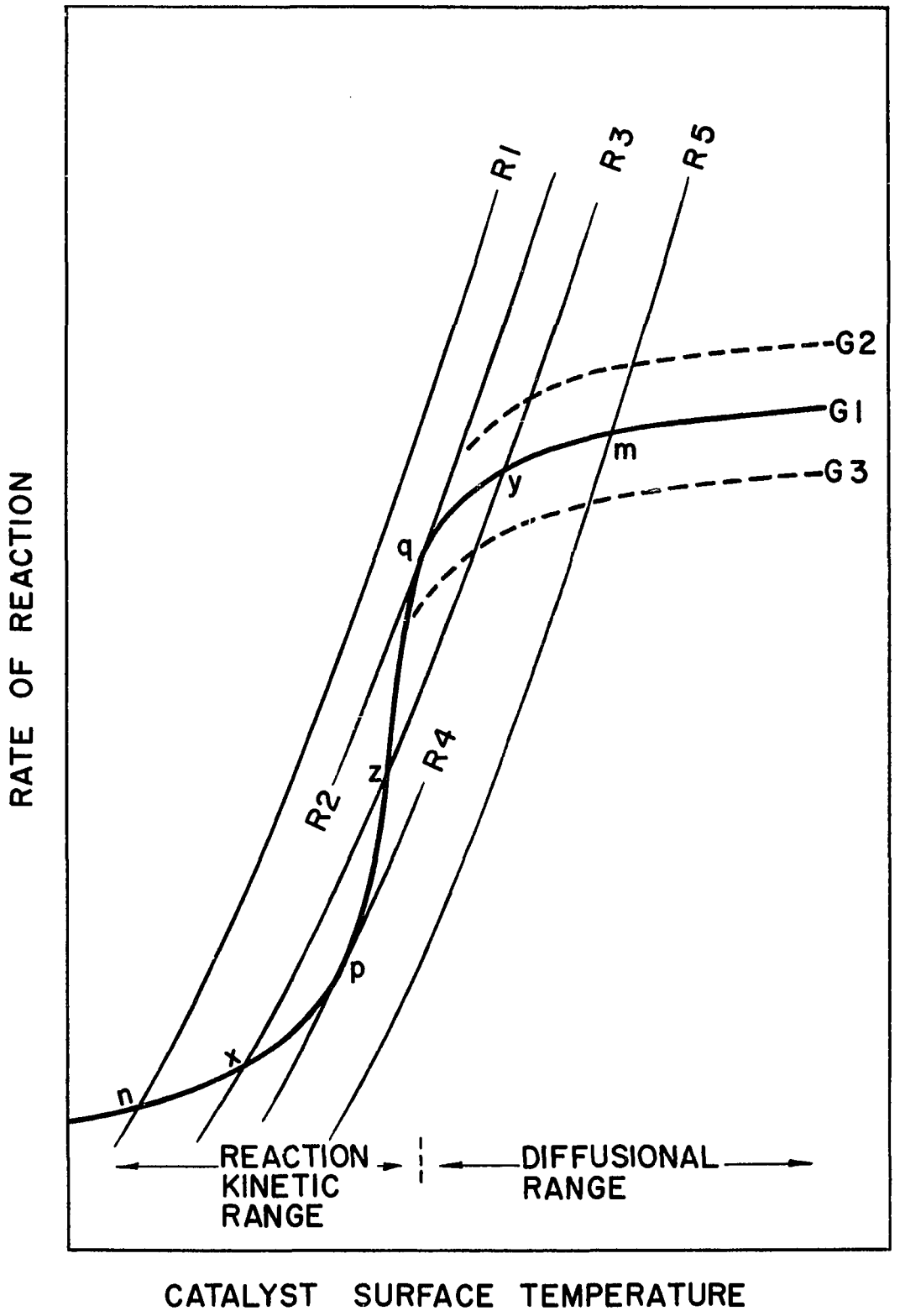

Figure 8 - Thermal Regime of the Catalyst Surface

surface temperature increase in the reaction kinetic range (lower thermal regime). For heat removal curve R5, the only stationary state possible is point m, corresponding to a large surface temperature increase in the diffusional range.

For heat removal curve R3 and heat generation curve G1, three stationary states are possible, of which, however, only the upper and lower are stable. Which stationary state will become established in this region depends upon the initial state of the surface. If the surface were at a high temperature and then placed in a cooler gas with a heat removal curve corresponding to R3, its temperature would drop only as far as the temperature corresponding to the upper intersection (point y) and would not fall any farther; i.e., the upper stationary state would be established.

Next, consider a reaction operating at the lower stationary state point n. If the heat removal curve were moved to the right (intensity of heat removal decreased), the temperature rise at the surface and the rate of reaction would increase continuously from point n, through point x, up to point p. On passing the point of contact p of the heat generation and removal curves, R4 and G1, a discontinuous change of the surface temperature rise and observed reaction rate would occur. The condition at which the heat generation and heat removal curves contact at point p is the condition of ignition of the solid body.

Finally, consider a reaction operating in the upper thermal regime at point m. If the intensity of heat removal is increased, the temperature rise at the surface and the observed rate of reaction would decrease continuously from point m, through point y, and down to point q.

With a further increase in intensity of heat removal beyond point q, there would be an abrupt drop of the temperature of the surface, and the reaction process would pass to the lower stationary state (point n) corresponding to a small temperature rise in the kinetic region.

In summary, for an exothermic heterogeneous reaction there can exist two stationary thermal states, one corresponding to a small temperature rise in the kinetic region (lower thermal regime), and the other corresponding to a large temperature rise in the diffusional region (upper thermal regime). Passage from one regime to the other occurs discontinuously at the critical conditions of surface ignition and extinction.

APPENDIX B

SMOOTHED REACTION RATE DATA

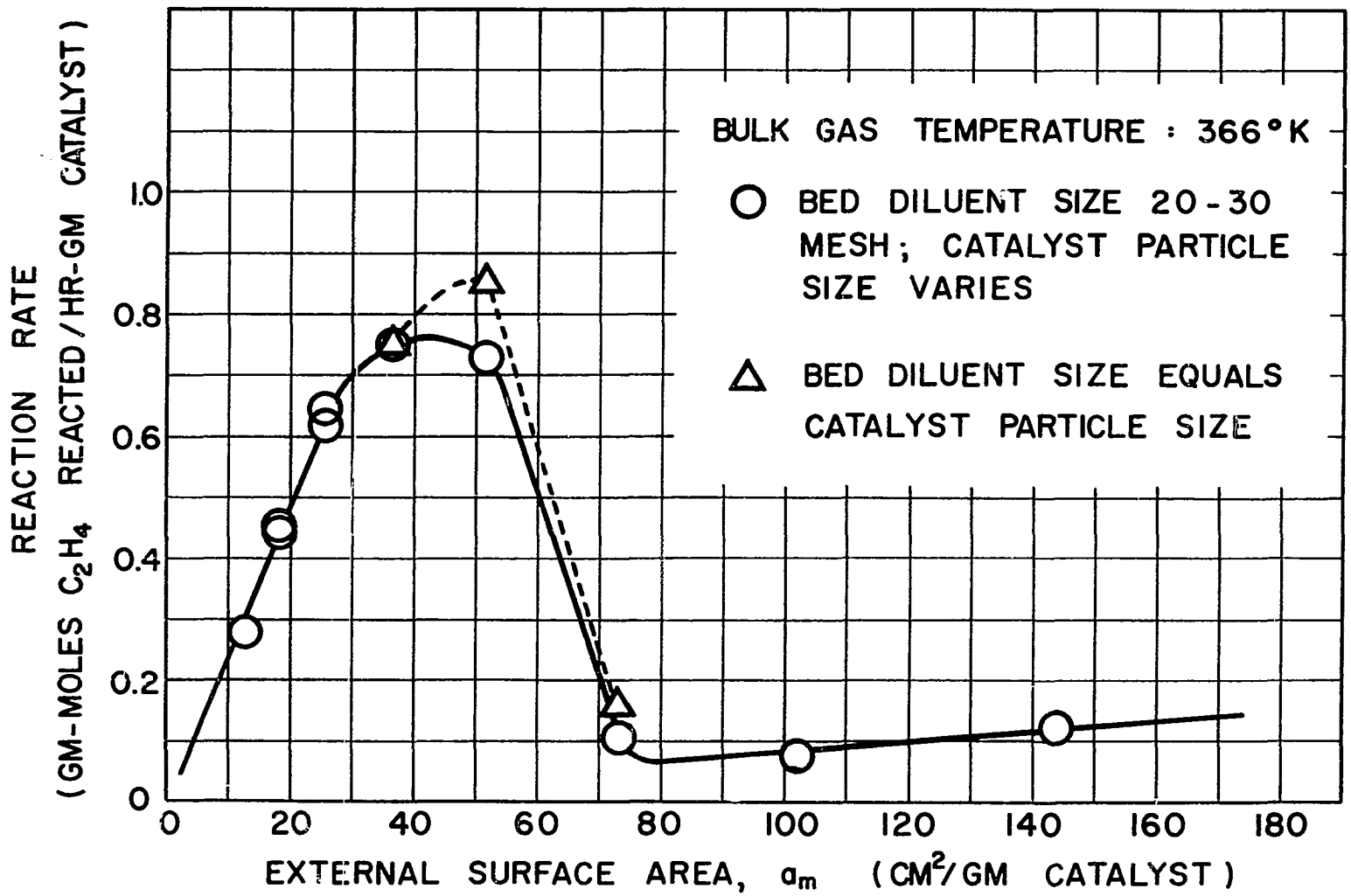

Figure 9 - Smoothed Reaction Rate Data at 366°K

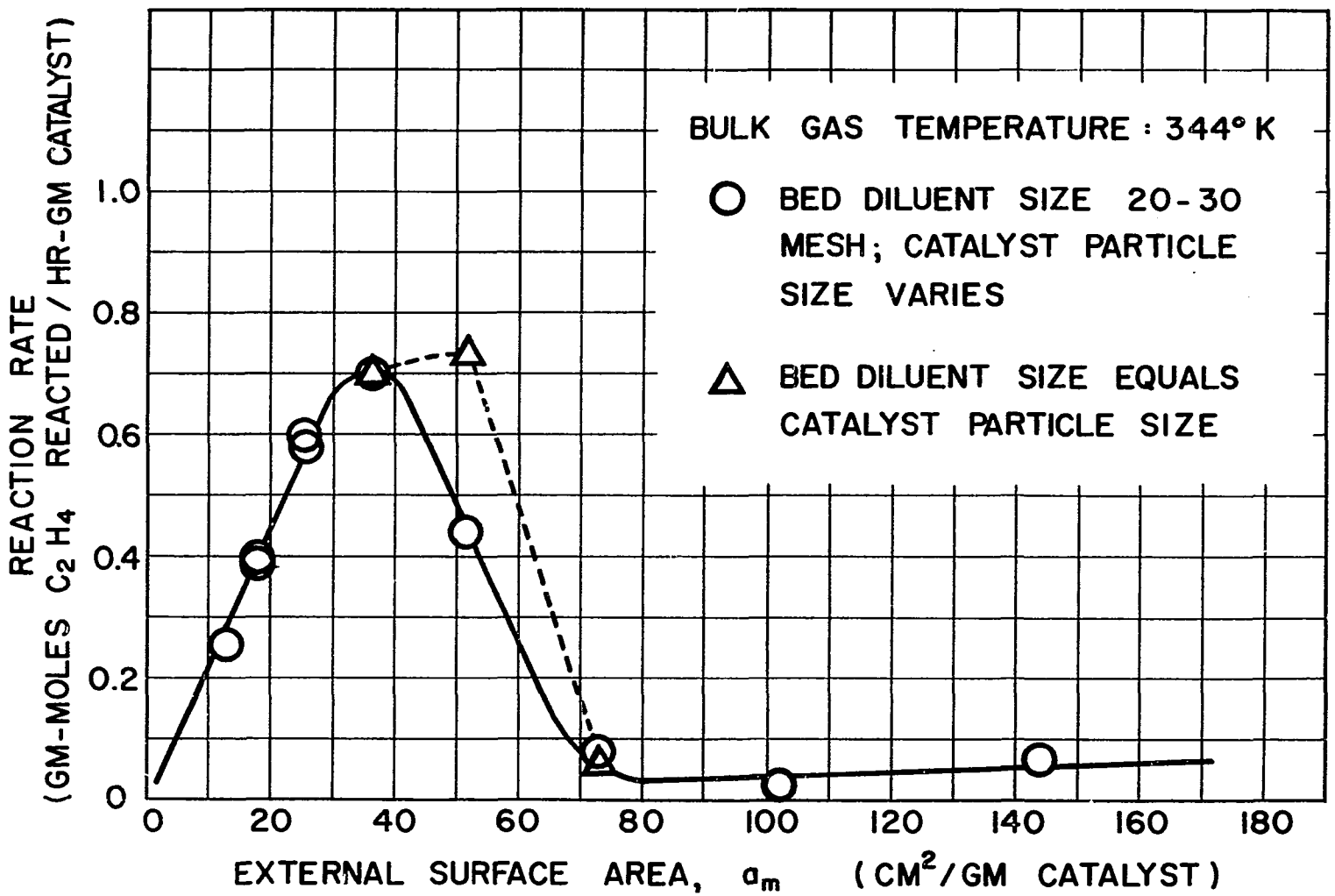

Figure 10 - Smoothed Reaction Rate Data at 344°K

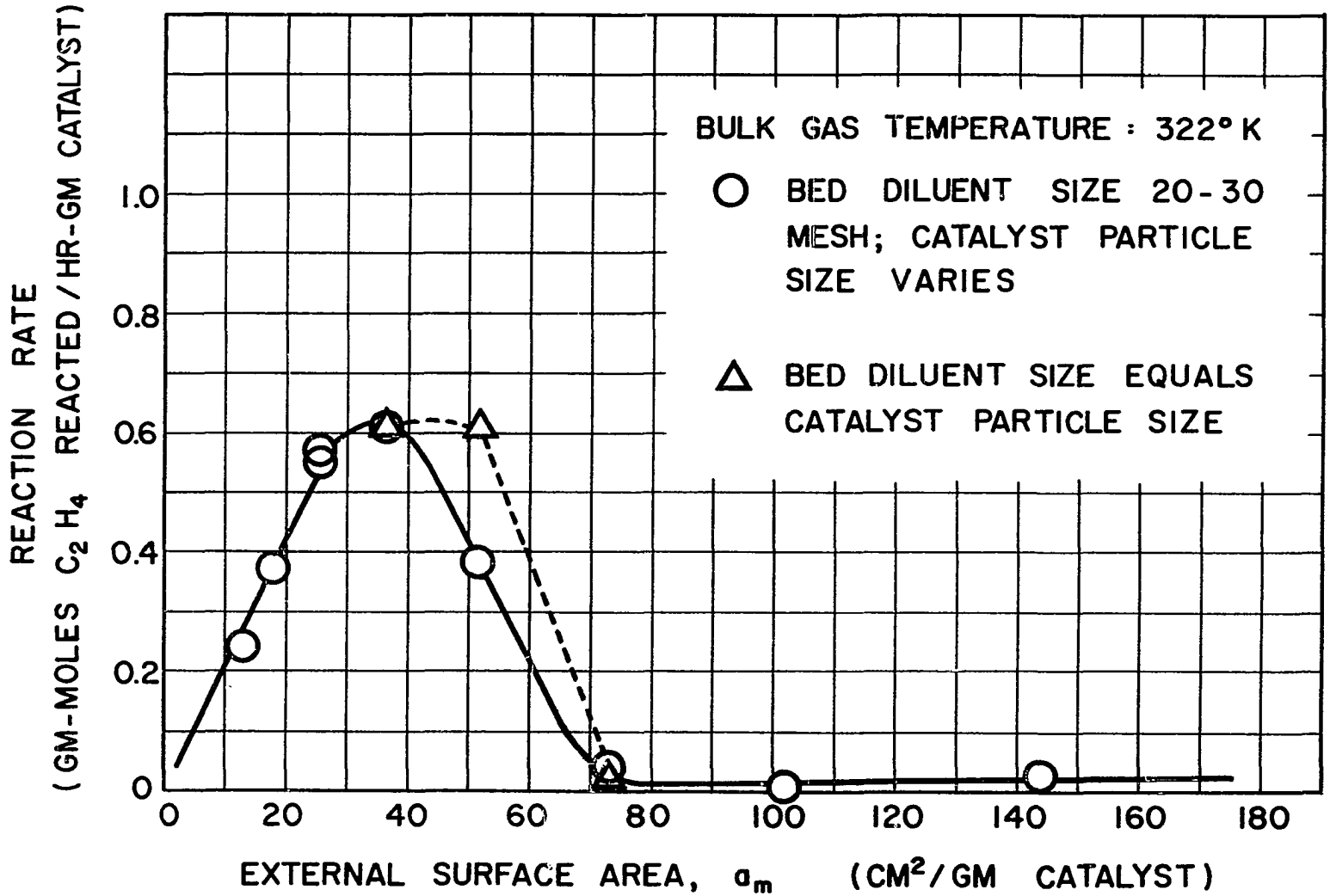

Figure 11 - Smoothed Reaction Rate Data at 322°K

APPENDIX C

SAMPLE CALCULATIONS OF θ AND γ

APPENDIX C

SAMPLE CALCULATIONS OF β AND γ

$$\beta = \left[\frac{\Delta H}{\rho C_{p_M} G_M} \cdot \frac{1}{(0.584)} \left(\frac{G_m}{\mu} \right)^{0.30} \left(\frac{C_{p_m} \mu}{k} \right)_f^{2/3} \right] \qquad \text{(VII-8)}$$

$$\gamma = \left[\frac{P_f}{\rho G_M} \cdot \frac{1}{(0.426)} \left(\frac{G_m}{\mu} \right)^{0.30} \left(\frac{\mu}{\rho_g D_i} \right)_f^{2/3} \right] \qquad \text{(VII-6)}$$

β and γ were calculated as functions of catalyst surface temperatures for a given bulk gas temperature. The average gas film temperature existing between the bulk gas phase and the catalyst surface was assumed to be the arithmetic average of the bulk phase and catalyst surface temperatures.

It was assumed that the physical properties of ethylene and ethane could be considered the same for the calculation of β and γ. A comparison of their various physical properties establishes this assumption as reasonable. Also, they occur in small concentrations with respect to the hydrogen (for entering feed, C_2H_4:H_2 = 1:4). Such a simplification eliminates the need to calculate the physical properties of the gas mixture as a function of degree of conversion.

Series of values of β and γ were calculated for each bulk temperature used in this study (322°K, 344°K, and 366°K). These calculated functions were plotted in order to be used with the trial and error

solutions of Equations (VII-5) and (VII-7).

A sample calculation of β and γ from the estimated calculated, or known system and physical properties is given below.

Temperature

$$T_{atm} = 300^{\circ}K$$

$$T_B = 366^{\circ}K$$

$$T_S = 566^{\circ}K$$

$$T_f = \frac{566 + 366}{2} = 466^{\circ}K$$

Reactor Cross-sectional Area

$$A_{cs} = 2.94 \text{ cm}^2$$

Flow Rate

$$G_{M_{H_2}} = \frac{8 \text{ cm}^3 H_2}{\text{sec}} \left| \frac{3600 \text{ sec}}{\text{hr}} \right| \frac{\text{gm-mole}}{22{,}414 \text{ cm}^3} \left| \frac{273^{\circ}K}{300^{\circ}K} \right| \frac{}{2.94 \text{ cm}^2}$$

$$= 0.398 \text{ gm-moles } H_2/\text{cm}^2 \text{ hr}$$

$$G_{M_{C_2H_4}} = \frac{2 \text{ cm}^3 C_2H_4}{\text{sec}} \left| \frac{3600 \text{ sec}}{\text{hr}} \right| \frac{\text{gm-mole}}{22{,}414 \text{ cm}^3} \left| \frac{273^{\circ}K}{300^{\circ}K} \right| \frac{}{2.94 \text{ cm}^2}$$

$$= 0.100 \text{ gm-moles/cm}^2 \text{ hr}$$

$$G_{M_{total}} = 0.498 \text{ gm-moles/cm}^2 \text{ hr}$$

$$G_{m_{H_2}} = \frac{0.398 \text{ gm-moles } H_2}{\text{hr cm}^2} \left| \frac{2 \text{ gm } H_2}{\text{gm-mole } H_2} \right. = 0.796 \text{ gm } H_2/\text{hr cm}^2$$

$$G_{m_{C_2H_4}} = \frac{0.100 \text{ gm-moles } C_2H_4}{\text{hr cm}^2} \left| \frac{28 \text{ gm } C_2H_4}{\text{gm-mole } C_2H_4} \right. = 2.80 \text{ gm } C_2H_4/\text{hr cm}^2$$

$$G_{m_{total}} = 3.6 \text{ gm/hr cm}^2 = \frac{3.6 \text{ gm}}{\text{hr cm}^2} \Big| \frac{\text{hr}}{3600 \text{ sec}} = 0.001 \text{ gm/sec cm}^2$$

Molal Heat Capacity (30)

$$C_{p_{H_2}} = 6.946 - (0.196 \times 10^{-3})T + (0.4757 \times 10^{-6})T^2$$

$$\left(C_{p_{H_2}}\right)_{466^\circ K} = 6.946 - (0.196 \times 10^{-3})(466) + (0.4757 \times 10^{-6})(466)^2$$

$$= 6.96 \text{ cal/gm-mole } ^\circ K$$

$$C_{p_{C_2H_4}} = 3.019 + (28.21 \times 10^{-3})T - (8.537 \times 10^{-6})T^2$$

$$\left(C_{p_{C_2H_4}}\right)_{466^\circ K} = 3.019 + (28.21 \times 10^{-3})(466) - (8.537 \times 10^{-6})(466)^2$$

$$= 14.51 \text{ cal/gm-mole } ^\circ K$$

$$\left(C_{p_{ave}}\right)_{466^\circ K} = 0.8(6.96) + 0.2(14.51) = 8.46 \text{ cal/gm-mole } ^\circ K$$

Heat of Reaction (30)

$C_2H_4 + 3O_2$	$\longrightarrow$	$2CO_2 + 2H_2O$	-337.234 kcal/gm-mole
$H_2 + \frac{1}{2}O_2$	$\longrightarrow$	H_2O	-68.317 kcal/gm-mole
$2CO_2 + 3H_2O$	$\longrightarrow$	$C_2H_6 + 3\frac{1}{2}O_2$	$+372.820$ kcal/gm-mole
$C_2H_4 + H_2$	$\longrightarrow$	C_2H_6	-32.731 kcal/gm-mole

$$\Delta H_{T_2} = \Delta H_o + \left[\left(C_{p_M}\right)_{mvP} - \left(C_{p_M}\right)_{mvR}\right](T_2 - T_o)$$

$$(\Delta H)_{566^\circ K} = -32{,}731 + (16.72 - 13.65 - 6.97)(566 - 298)$$

$= -33{,}811$ cal/gm-mole

Gas Density

$$(\rho_g)_{466^\circ K} = \frac{0.0877}{466} = 1.88 \times 10^{-4} \text{ gm/cm}^3$$

Shape Factor (22)

Spheres	$\phi = 1.0$
Cylinders	$\phi = 0.91$
Irregular granules	$\phi = 0.90$ (assumed)
Flakes	$\phi = 0.81$

Viscosity (30)(47)

$(T_c)_{H_2} = 33.3^\circ K$ $\qquad (T_c)'_{H_2} = 0.8(33.3) = 26.64^\circ K$

$(T_c)_{C_2H_4} = 283.1^\circ K$ $\qquad (T_c)'_{C_2H_4} = 0.2(283.1) = \underline{56.62^\circ K}$

$T_c' = 83.26^\circ K$

$$T_r' = \frac{T}{T_c'} = \frac{466^\circ K}{83.26^\circ K} = 5.70$$

$(p_c)_{H_2} = 12.8$ atm $\qquad (p_c)'_{H_2} = 0.8(12.8) = 10.24$ atm

$(p_c)_{C_2H_4} = 50.50$ atm $\qquad (p_c)'_{C_2H_4} = 0.2(50.50) = \underline{10.10 \text{ atm}}$

p_c' $\qquad 20.34$ atm

$$p_r' = \frac{p}{p_c'} = \frac{1}{20.34} = 0.492$$

$\mu_r' = 1.76$

$(\mu_c)_{H_2} = 34.7 \times 10^{-6}$ poise $\qquad 0.8(34.7 \times 10^{-6}) = 27.7 \times 10^{-6}$ poise

$(\mu_c)_{C_2H_4} = 215 \times 10^{-6}$ poise $\qquad 0.2(215 \times 10^{-6}) = \underline{43.0 \times 10^{-6} \text{ poise}}$

70.7×10^{-6} poise

$$\mu_{466^\circ K} = \mu_r' \mu_c' = 1.76(70.7 \times 10^{-6}) = 124 \times 10^{-6} \text{ poise}$$

Diffusion Coefficient (26)(47)

Assume diffusion of C_2H_4 in H_2 is important, since there is always a large excess of H_2. The application of the Lennard-Jones potential by Hirschfelder, Curtiss and Bird has been most generally employed to predict diffusion coefficients.

C_2H_4 $\begin{cases} \sigma_1 = 4.232 \\ \frac{\epsilon_1}{k} \quad 205 \end{cases}$ H_2 $\begin{cases} \sigma_2 = 2.968 \\ \frac{\epsilon_2}{k} = 33.3 \end{cases}$

$$\sigma_{12} = \frac{4.232 + 2.968}{2} = 3.6$$

$$(\sigma_{12})^2 = 13.0$$

$$\frac{\epsilon_{12}}{k} = \frac{\sqrt{\epsilon_1 \epsilon_2}}{k} = \sqrt{33.3(205)} = 82.5$$

at 466^oK, $\frac{kt}{\epsilon_{12}} = 5.74$, $\Omega_D = 0.8180$

$$D_{12} = \frac{0.001858T^{3/2}\left[(M_1 + M_2)/M_1M_2\right]^{1/2}}{\pi \sigma_{12}^2 \Omega_D}$$

$$= \frac{0.001858(466)^{3/2}\left[(28 + 2)/28(2)\right]^{1/2}}{1\ (13.0)\ 0.8180}$$

$$= 1.31\ cm^2/sec$$

Prandtl Number

The Prandtl number is independent of temperature within the range of this study.

$(Pr)_{H_2}$, $366^oK = 0.74$

$(Pr)_{C_2H_4}$, $366^oK = 0.83$

$$(Pr)_{ave} \; ; \quad 366^{\circ}K = 0.8(0.74) + 0.2(0.83) = 0.758$$

$$(Pr)^{2/3}_{ave} = 0.833$$

For Denton's correlation the Prandtl number was 0.73. For gases the range of Prandtl number is $0.6 < Pr < 1.0$.

Schmidt Number

$$\left(\frac{\mu}{\rho_g D_i}\right)^{2/3}_{466^{\circ}K} = \left(\frac{124 \times 10^{-6} \; \cancel{gm} \,/\, \cancel{cm}\,\cancel{sec}}{1.88 \times 10^{-4} \; \cancel{gm} \,/\, \cancel{cm^3}} \cdot \frac{\cancel{cm^2}}{1.31 \; \cancel{sec}}\right)^{2/3}$$

$$= (0.505)^{2/3} = 0.638$$

For gases the range of the Schmidt number is $0.5 < Sc < 2.0$.

Pressure Factor, p_f

For diffusion through a stagnant film in binary gas mixtures, the pressure factor p_f is the logarithmic mean value of the partial pressure of the non-diffusing gas at the surface and in the bulk gas stream.

C_2H_4 +	H_2 ⟶	C_2H_6
$(0.2 - y)$	$(0.8 - y)$	(y)
Total number of moles		$0.2 - y$ $0.8 - y$ y $1 - y$

Partial pressure of hydrogen $\quad \frac{0.8 - y}{1 - y}\pi = p_{H_2}$

At complete conversion, $p_{H_2} \quad \frac{0.8 - 0.2}{1 - 0.2}\pi = \frac{0.6}{0.8} = 0.75$ atm

At no conversion, $p_{H_2} \quad \frac{0.8 - 0}{1 - 0}\pi = 0.8$

Since the widest range of hydrogen partial pressure possible is 0.8 to

0.75 atm, the value of the partial pressure factor actually encountered will be relatively constant and assumed to be a constant 0.8 atm.

Temperature Group, β

$$\beta_{566^{\circ}K} = \frac{33{,}811 \text{ cal}}{\text{gm-mole}} \left| \; 0.9 \; \right| \frac{\text{gm-mole } ^{\circ}K}{8.46 \text{ cal}} \left| \; 0.498 \text{ gm-moles} \; \right| \frac{\text{cm}^2 \text{ hr}}{} \left| \; 0.584 \right.$$

$$X \left(\frac{0.001 \text{ gm}}{\text{sec cm}^2} \middle| \frac{\text{cm sec}}{124 \times 10^{-6} \text{ gm}} \right)^{0.30} \quad (0.833)$$

$$= 23{,}600^{\circ}K \text{ cm}^2 \text{ hr cm}^{-0.3} \text{ gm-mole}^{-1}$$

Diffusion Group, γ

$$\gamma_{566^{\circ}K} = \frac{0.8 \text{ atm}}{} \left| \; 0.9 \; \right| \frac{\text{cm}^2 \text{ hr}}{0.498 \text{ gm-moles}} \left| \; 0.426 \right.$$

$$X \left(\frac{0.001 \text{ gm}}{\text{sec cm}^2} \middle| \frac{\text{cm sec}}{124 \times 10^{-6} \text{ gm}} \right)^{0.30} \quad (0.505)^{2/3}$$

$$= 5.00 \text{ atm cm}^2 \text{ hr cm}^{-0.3} \text{ gm-mole}^{-1}$$

APPENDIX D

SAMPLE CALCULATION OF ARRHENIUS RATE CONSTANT

APPENDIX D

SAMPLE CALCULATION OF ARRHENIUS RATE CONSTANT

Arrhenius rate constant: $k = Ae^{-\Delta H^*/RT}$

Literature rate equation: $\frac{r_m}{a_m} = k(P_{H_2})_S \, (P_{C_2H_4})_S$

Bulk stream partial pressure: $(P_{H_2})_B = 0.8$ atm

$(P_{C_2H_4})_B = 0.2$ atm

Partial pressure gradient: Δp (for both H_2 and C_2H_4)

Actual surface concentration: $(P_{H_2})_S = (0.8 - \Delta p)$ atm

$(P_{C_2H_4})_S = (0.2 - \Delta p)$ atm

$$k = \frac{r_m/a_m}{(0.8 - \Delta p)(0.2 - \Delta p)} = Ae^{-\Delta H^*/RT}$$

For 12-16 mesh catalyst

$T_B = 366^oK$

$G_M = 0.498$ gm-moles/hr cm^2

$$k = \frac{0.0242}{(0.8 - 0.0714)(0.2 - 0.0714)}$$

$= 0.258$ gm-moles/hr cm^2 atm^2

APPENDIX E

CHROMATOGRAPH CALIBRATION

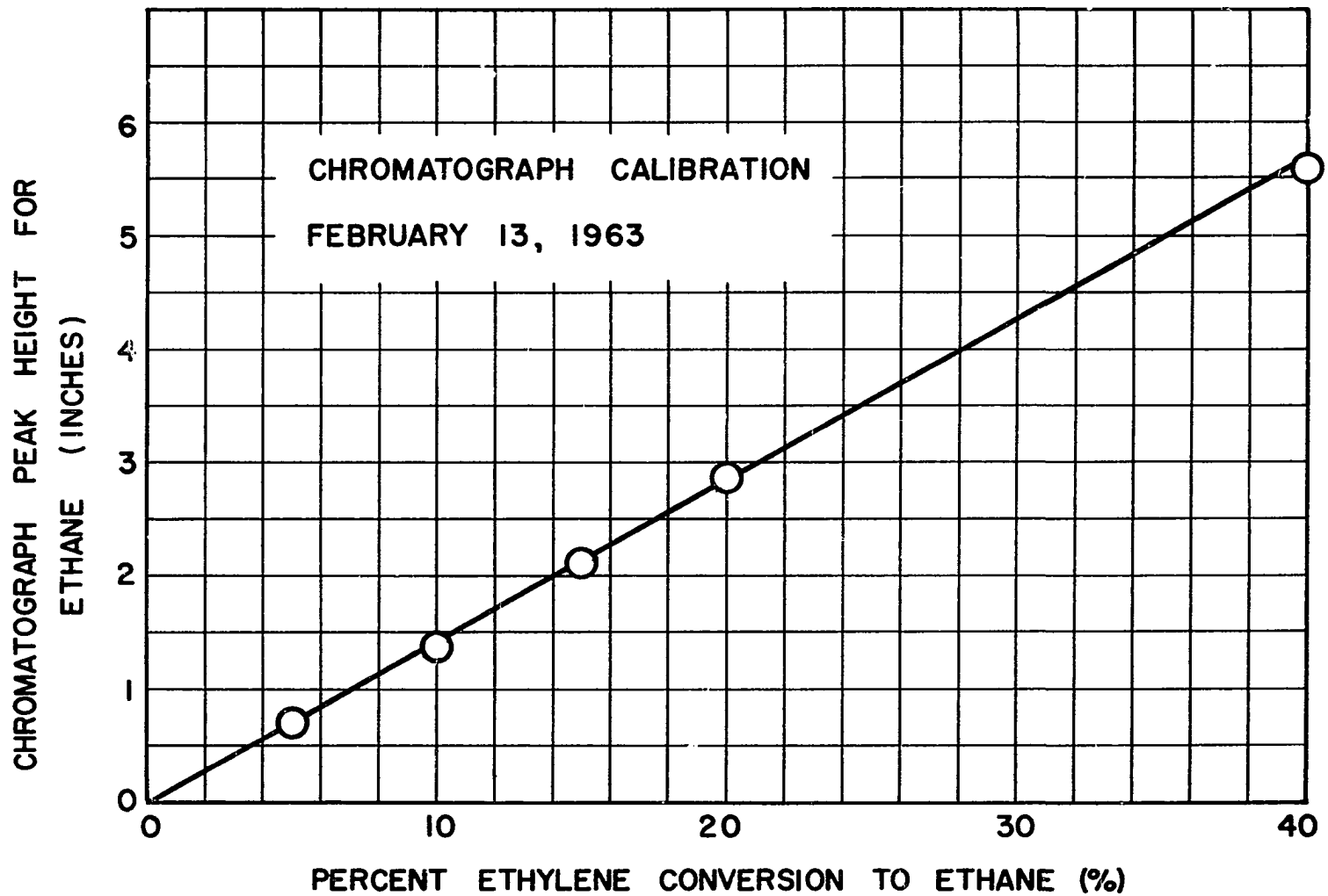

Figure 12 - Chromatograph Calibration

EXPERIMENTAL DATA

Run Number 8 Date 2/25/63

Catalyst

Mesh Size (U. S. Standard) 8-12

Particle Diameter (cm) 0.2030

Sample Weight (grams) 0.2 (23 pellets)

Diluent: 100 ml 20-30 mesh Ottawa sand

Temp.	Ethylene Flow Rate		Hydrogen Flow Rate		Δp	$\frac{W}{F}$	Conv.
(°F)	(cc/sec)	(g-m/hr)	(cc/sec)	(g-m/hr)	(in.TEG)		(%)
197	2	0.292	8	1.168	2.5	0.685	22
	4	0.584	16	2.336	5.3	0.343	12
	6	0.876	24	3.504	8.0	0.228	8.5
162	2	0.292	8	1.168	2.4	0.685	20
	4	0.584	16	2.336	4.9	0.343	11
	6	0.876	24	3.504	7.3	0.228	7.5
120	2	0.292	8	1.168	2.0	0.685	19
	4	0.584	16	2.336	4.3	0.343	10
	6	0.876	24	3.504	6.7	0.228	7.0

Run Number 10 Date 2/28/63

Catalyst

Mesh Size (U. S. Standard) 12-16

Particle Diameter (cm) 0.1435

Sample Weight (grams) 0.1 (29 pellets)

Diluent: 100 ml 20-30 mesh Ottawa sand

Temp.	Ethylene Flow Rate		Hydrogen Flow Rate		ΔP	$\frac{W}{F}$	Conv.
(°F)	(cc/sec)	(g-m/hr)	(cc/sec)	(g-m/hr)	(in.TEG)		(%)
199	2	0.292	8	1.168	2.5	0.343	15.0
	4	0.584	16	2.336	5.3	0.171	7.5
	6	0.876	24	3.504	7.8	0.114	5.2
161	2	0.292	8	1.168	2.2	0.343	14.0
	4	0.584	16	2.336	4.7	0.171	7.3
	6	0.876	24	3.504	7.1	0.114	5.0
120	2	0.292	8	1.168	2.1	0.343	12.7
	4	0.584	16	2.336	4.1	0.171	6.9
	6	0.876	24	3.504	6.3	0.114	4.9

Run Number 9 Date 2/26/63

Catalyst

Mesh Size (U. S. Standard) 12-16

Particle Diameter (cm) 0.1435

Sample Weight (grams) 0.2 (54 pellets)

Diluent: 100 ml 20-30 mesh Ottawa sand

Temp.	Ethylene Flow Rate		Hydrogen Flow Rate		ΔP	$\frac{W}{F}$	Conv.
(°F)	(cc/sec)	(g-m/hr)	(cc/sec)	(g-m/hr)	(in.TEG)		(%)
194	2	0.292	8	1.168	2.3	0.685	34
	4	0.584	16	2.336	5.0	0.343	19
	6	0.876	24	3.504	7.5	0.228	14
160	2	0.292	8	1.168	2.2	0.685	31
	4	0.584	16	2.336	4.6	0.343	18
	6	0.876	24	3.504	6.9	0.228	13
118	2	0.292	8	1.168	1.9	0.685	29
	4	0.584	16	2.336	4.2	0.343	16
	6	0.876	24	3.504	6.3	0.228	12

Run Number 11 Date 3/1/63

Catalyst

Mesh Size (U. S. Standard) 16-20

Particle Diameter (cm) 0.1015

Sample Weight (grams) 0.1 (78 particles)

Diluent: 100 ml 20-30 mesh Ottawa sand

Temp.	Ethylene Flow Rate		Hydrogen Flow Rate		ΔP	$\frac{W}{F}$	Conv.
(°F)	(cc/sec)	(g-m/hr)	(cc/sec)	(g-m/hr)	(in.TEG)		(%)
198	2	0.292	8	1.168	2.5	0.343	22.5
	4	0.584	16	2.336	5.3	0.171	12.0
	6	0.876	24	3.504	7.8	0.114	8.5
158	2	0.292	8	1.168	2.2	0.343	20.5
	4	0.584	16	2.336	4.7	0.171	11.0
	6	0.876	24	3.504	7.1	0.114	7.6
120	2	0.292	8	1.168	2.1	0.343	19.4
	4	0.584	16	2.336	4.2	0.171	10.0
	6	0.876	24	3.504	6.4	0.114	7.0

Run Number 12 Date 3/2/63

Catalyst

Mesh Size (U. S. Standard) 16-20

Particle Diameter (cm) 0.1015

Sample Weight (grams) 0.2 (151 particles)

Diluent: 100 ml 20-30 mesh Ottawa sand

Temp.	Ethylene Flow Rate		Hydrogen Flow Rate		$\triangle P$	$\frac{W}{F}$	Conv.
(°F)	(cc/sec)	(g-m/hr)	(cc/sec)	(g-m/hr)	(in.TEG)		(%)
200	2	0.292	8	1.168	2.5	0.685	60
	4	0.584	16	2.336	5.3	0.343	36.6
	6	0.876	24	3.504	7.8	0.228	27.4
165	2	0.292	8	1.168	2.2	0.685	56
	4	0.584	16	2.336	4.7	0.343	34
	6	0.876	24	3.504	7.1	0.228	26.1
122	2	0.292	8	1.168	2.1	0.685	53.2
	4	0.584	16	2.336	4.2	0.343	32
	6	0.876	24	3.504	6.4	0.228	24.1

Run Number 13 Date 3/4/63

Catalyst

Mesh Size (U. S. Standard) 20-30

Particle Diameter (cm) 0.0715

Sample Weight (grams) 0.1

Diluent: 100 ml 20-30 mesh Ottawa sand

Temp.	Ethylene Flow Rate		Hydrogen Flow Rate		$\triangle P$	$\frac{W}{F}$	Conv.
(°F)	(cc/sec)	(g-m/hr)	(cc/sec)	(g-m/hr)	(in.TEG)		(%)
199	2	0.292	8	1.168	2.5	0.343	27.7
	4	0.584	16	2.336	5.3	0.171	14.7
	6	0.876	24	3.504	7.8	0.114	10.3
162	2	0.292	8	1.168	2.2	0.343	25.6
	4	0.584	16	2.336	4.7	0.171	13.4
	6	0.876	24	3.504	7.1	0.114	9.5
118	2	0.292	8	1.168	2.1	0.343	22.0
	4	0.584	16	2.336	4.2	0.171	11.5
	6	0.876	24	3.504	6.4	0.114	8.2

Run Number 14 Date 3/5/63

Catalyst

Mesh Size (U. S. Standard) 30-40

Particle Diameter (cm) 0.0505

Sample Weight (grams) 0.1

Diluent: 100 ml 20-30 mesh Ottawa sand

Temp.	Ethylene Flow Rate		Hydrogen Flow Rate		ΔP	$\frac{W}{F}$	Conv.
(^{o}F)	(cc/sec)	(g-m/hr)	(cc/sec)	(g-m/hr)	(in.TEG)		(%)
203	2	0.292	8	1.168	2.5	0.343	18.4
	4	0.584	16	2.336	5.3	0.171	9.5
	6	0.876	24	3.504	7.8	0.114	6.5
157	2	0.292	8	1.168	2.2	0.343	15.4
	4	0.584	16	2.336	4.7	0.171	8.2
	6	0.876	24	3.504	7.1	0.114	5.7
122	2	0.292	8	1.168	2.1	0.343	13.7
	4	0.584	16	2.336	4.2	0.171	6.7
	6	0.876	24	3.504	6.4	0.114	4.8

Run Number 16 Date 3/8/63

Catalyst

Mesh Size (U. S. Standard) 30-40

Particle Diameter (cm) 0.0505

Sample Weight (grams) 0.1

Diluent: 100 ml 30-40 mesh Ottawa sand

Temp.	Ethylene Flow Rate		Hydrogen Flow Rate		ΔP	$\frac{W}{F}$	Conv.
(^{o}F)	(cc/sec)	(g-m/hr)	(cc/sec)	(g-m/hr)	(in.TEG)		(%)
202	2	0.292	8	1.168	4.3	0.343	28.0
	4	0.584	16	2.336	9.0	0.171	13.6
	6	0.876	24	3.504	13.7	0.114	10.0
164	2	0.292	8	1.168	3.6	0.343	25.1
	4	0.584	16	2.336	8.2	0.171	12.8
	6	0.876	24	3.504	12.3	0.114	8.4
120	2	0.292	8	1.168	3.4	0.343	20.8
	4	0.584	16	2.336	7.1	0.171	10.6
	6	0.876	24	3.504	10.8	0.114	7.0

Run Number 28 Date 7/10/63

Catalyst

Mesh Size (U. S. Standard) 40-50

Particle Diameter (cm) 0.0358

Sample Weight (grams) 0.1

Diluent: 100 ml 20-30 mesh Ottawa sand

Temp.	Ethylene Flow Rate		Hydrogen Flow Rate		ΔP	W/F	Conv.
(°F)	(cc/sec)	(g-m/hr)	(cc/sec)	(g-m/hr)	(in.TEG)		(%)
200	2	0.292	8	1.168	2.5	0.343	3.7
	4	0.584	16	2.336	5.3	0.171	1.8
	6	0.876	24	3.504	7.8	0.114	1.4
163	2	0.292	8	1.168	2.2	0.343	2.5
	4	0.584	16	2.336	4.7	0.171	1.4
	6	0.876	24	3.504	7.1	0.114	1.0
123	2	0.292	8	1.168	2.1	0.343	1.4
	4	0.584	16	2.336	4.2	0.171	0.7
	6	0.876	24	3.504	6.4	0.114	0.35
203	1	0.146	4	0.584		0.686	4.4
	½	0.073	2	0.292		1.372	7.5
	¼	0.036	1	0.146		2.744	15.7

Run Number 17 Date 3/11/63

Catalyst

Mesh Size (U. S. Standard) 40-50

Particle Diameter (cm) 0.0358

Sample Weight (grams) 0.1

Diluent: 100 ml 40-50 mesh Ottawa sand

Temp.	Ethylene Flow Rate		Hydrogen Flow Rate		ΔP	$\frac{W}{F}$	Conv.
(°F)	(cc/sec)	(g-m/hr)	(cc/sec)	(g-m/hr)	(in.TEG)		(%)
199	1	0.146	4	0.584	3.7	0.685	10.5
	2	0.292	8	1.168	7.8	0.343	5.1
	3	0.438	12	1.752	12.2	0.228	3.2
160	1	0.146	4	0.584	3.5	0.685	4.3
	2	0.292	8	1.168	6.9	0.343	1.7
	3	0.438	12	1.752		0.228	1.0
123	1	0.146	4	0.584	2.6	0.685	1.7
	2	0.292	8	1.168	6.4	0.343	0.6
	3	0.438	12	1.1752	9.7	0.228	0.4

Run Number 25 Date 3/28/63

Catalyst

Mesh Size (U. S. Standard) 50-70

Particle Diameter (cm) 0.0254

Sample Weight (grams) 0.2

Diluent: 100 ml 20-30 mesh Ottawa sand and glass wool

Temp.	Ethylene Flow Rate		Hydrogen Flow Rate		ΔP	$\frac{W}{F}$	Conv.
(^{o}F)	(cc/sec)	(g-m/hr)	(cc/sec)	(g-m/hr)	(in.TEG)		(%)
198	2	0.292	8	1.168	2.5	0.685	5.3
154	2	0.292	8	1.168	2.3	0.685	1.6
123	2	0.292	8	1.168	2.1	0.685	0.3

Run Number 22 Date 3/22/63

Catalyst

Mesh Size (U. S. Standard) 70-100

Particle Diameter (cm) 0.0180

Sample Weight (grams) 0.1

Diluent: 100 ml 20-30 mesh Ottawa sand and glass wool

Temp.	Ethylene Flow Rate		Hydrogen Flow Rate		ΔP	$\frac{W}{F}$	Conv.
(°F)	(cc/sec)	(g-m/hr)	(cc/sec)	(g-m/hr)	(in.TEG)		(%)
199	2	0.292	8	1.168	2.4	0.343	4.1
	4	0.584	16	2.336	4.9	0.171	2.0
	6	0.876	24	3.504	7.1	0.114	1.5
156	2	0.292	8	1.168	2.0	0.343	2.7
	4	0.584	16	2.336	4.2	0.171	1.0
	6	0.876	24	3.504	6.3	0.114	0.7
120	2	0.292	8	1.168	1.8	0.343	1.5
	4	0.584	16	2.336	3.8	0.171	0.6
	6	0.876	24	3.504	5.7	0.114	0.3

Run Number 23 Date 3/25/63

Catalyst

Mesh Size (U. S. Standard) 140-200

Particle Diameter (cm) 0.0090

Sample Weight (grams) 50 mg

Diluent: 100 ml 20-30 mesh Ottawa sand and glass wool

Temp.	Ethylene Flow Rate		Hydrogen Flow Rate		ΔP	$\frac{W}{F}$	Conv.
(°F)	(cc/sec)	(g-m/hr)	(cc/sec)	(g-m/hr)	(in.TEG)		(%)
199	2	0.292	8	1.168	2.5	0.171	4.8
	4	0.584	16	2.336	4.8	0.086	3.0
	6	0.876	24	3.504	7.3	0.057	2.4
159	2	0.292	8	1.168	2.1	0.171	4.5
119	2	0.292	8	1.168	1.9	0.171	2.4

Run Number 27 Date 4/1/63

Catalyst

Mesh Size (U. S. Standard) 200-325

Particle Diameter (cm) 0.0059

Sample Weight (grams) 0.1

Diluent: 100 ml 20-30 mesh Ottawa sand and glass wool

Temp.	Ethylene Flow Rate		Hydrogen Flow Rate		ΔP	$\frac{W}{F}$	Conv.
(^{o}F)	(cc/sec)	(g-m/hr)	(cc/sec)	(g-m/hr)	(in.TEG)		(%)
203	2	0.292	8	1.168	2.6	0.343	22.3
	4	0.584	16	2.336	4.8	0.171	19.2
	6	0.876	24	3.504	7.1	0.114	20.0
160	2	0.292	8	1.168	2.1	0.343	26.2
	4	0.584	16	2.336	4.3	0.171	20.2
	6	0.876	24	3.504	7.2	0.114	20.1
120	2	0.292	8	1.168	1.9	0.343	23.3
	4	0.584	16	2.366	3.9	0.171	17.3
	6	0.876	24	3.504	5.8	0.114	14.9

SUMMARY OF CALCULATIONS

SUMMARY OF CALCULATIONS

G_M = 0.498 gm-moles/cm^2 hr

Catalyst Mesh	8-12	12-16	16-20	20-30	30-40	40-50	50-70	70-100
Catalyst $(d_p)_{ave}$	.2030	.1435	.1015	.0715	.0505	.0358	.0254	.0180
Bed Diluent 20-30 Mesh Ottawa Sand								
T_B = 366°K								
$(r_m/a_m)_{exp'l} X\ 10^4$	217	247	246	206	102	14.9	7.58	8.35
$(r_m/a_m)_{smooth} X\ 10^4$	242	242	242	206	102	14.9	8.35	8.35
$\Delta p\ X\ 10^4$	792	714	640	493	226	29	1.46	1.40
ΔT	350	315	288	226	111	12	<1	<1
T_B = 344°K								
$(r_m/a_m)_{exp'l} X\ 10^4$	200	217	230	192	85.8	10.9	2.29	4.85
$(r_m/a_m)_{smooth} X\ 10^4$	223	223	223	192	85.8	10.9	3.88	3.88
$\Delta p\ X\ 10^4$	738	670	600	465	193	22.3	<1	<1
ΔT	321	294	264	206	104	10	<1	<1
T_B = 322°K								
$(r_m/a_m)_{exp'l} X\ 10^4$	190	206	218	168	74.5	5.62	0.43	2.76
$(r_m/a_m)_{smooth} X\ 10^4$	211	211	211	168	74.5	5.62	1.47	1.47
$\Delta p\ X\ 10^4$	710	640	574	412	169	11.1	<1	<1
ΔT	303	281	253	118	90	8	<1	<1
Bed Diluent Same Size as Catalyst Particle								
T_B = 366°K								
$(r_m/a_m)_{exp'l} X\ 10^4$				206	165	21.0		
T_B = 344°K								
$(r_m/a_m)_{exp'l} X\ 10^4$				192	141	7.65		
T_B = 322°K								
$(r_m/a_m)_{exp'l} X\ 10^4$				168	118	3.28		